A gradient border model for cell fate decisions at the neural plate border

Alexandre Thiery[1], Ailin Leticia Buzzi[1], Eva Hamrud[1], Chris Cheshire[2], Nicholas Luscombe[2#], James Briscoe[2], Andrea Streit[1*]

1 Centre for Craniofacial and Regenerative Biology, Faculty of Dentistry, Oral and Craniofacial Sciences, King's College London, London, UK.

2 Bioinformatics and Computational Biology Laboratory, The Francis Crick Institute, 1 Midland Road, London, UK.

Current address: Genomics and Regulatory Systems Unit, Okinawa Institute of Science and Technology Graduate University, Japan.

*Corresponding author: andrea.streit@kcl.ac.uk

Abstract

The vertebrate 'neural plate border' is a transient territory located at the edge of the neural plate containing precursors for all ectodermal derivatives: the neural plate; neural crest; placodes; and epidermis. Elegant functional experiments in a range of vertebrate models have provided an in-depth understanding of gene regulatory interactions within the ectoderm. However, these experiments conducted at tissue level raise seemingly contradictory models for fate allocation of individual cells. Here, we carry out single cell RNA sequencing of chick ectoderm from primitive streak to neurulation stage, to explore cell state diversity and heterogeneity. We characterise the dynamics of gene modules containing key factors known to regulate ectodermal cell fates, allowing us to model the order in which these fates are specified. Furthermore, we find that genes previously classified as neural plate border specifiers typically exhibit dynamic expression patterns and are biased towards either placodal or neural crest fates, revealing that the neural plate border should be seen as an anatomical region of the ectoderm and not a discrete transcriptional state. Through co-expression of placodal and neural crest markers, we identify a population of border located unstable progenitors (BLUPs) which gradually reduces in size as fate segregation occurs. Considering our findings, we propose a 'gradient border' model for cell fate choice at the neural plate border, with the probability of cell fate allocation closely tied to the spatiotemporal positioning of cells.

Introduction

The vertebrate nervous system is arguably the most complex organ of our body. During development, it arises from only three progenitor populations: the neural plate generates the entire central nervous system, while neural crest and sensory placodes jointly form the peripheral nervous system. Placode derivatives are confined to the head contributing to sense organs and cranial ganglia, while neural crest cells form along the entire body axis to generate various cell types including neurons and glial as well as parts of the craniofacial skeleton, cartilage and teeth (for review: Baker & Bronner-Fraser, 1997a; Baker & Bronner-Fraser, 2001; Grocott et al., 2012; Patthey et al., 2014; Pla & Monsoro-Burq, 2018; Prasad et al., 2019; Simoes-Costa & Bronner, 2015).

The neural plate becomes morphologically distinct shortly after gastrulation, although neural, neural crest and placode precursors continue to be intermingled at its edge, in a territory termed the neural plate border (NPB). The NPB has been characterised by the co-expression of neural and non-neural markers as well as so-called NPB specifiers (Pla & Monsoro-Burq, 2018; Roellig et al., 2017; Streit, 2002; Thiery et al., 2020). As the neural plate invaginates, placode precursors remain in the surface ectoderm, while neural crest cells are largely incorporated into neural folds from where they delaminate and migrate extensively. Although the induction of these three fates has been studied for decades, some of the most fundamental questions remain unresolved. For example, we do not know when and how these lineages segregate, whether they do so in a specific order and how individual cells make these decisions.

Modulation of different signalling pathways plays a crucial role in controlling the fate of all ectodermal cells. FGF signalling is required for the specification of neural, neural crest and placode precursors and for positioning the NPB (Ahrens & Schlosser, 2005; Litsiou et al., 2005; Londin et al., 2005; Monsoro-Burq et al., 2003; Streit et al., 2000; Streit & Stern, 1999; Stuhlmiller & García-Castro, 2012; Wilson et al., 2000; Yardley & Garcia-Castro, 2012). While BMP signalling must be inhibited for neural development (Hemmati-Brivanlou et al., 1994; Linker & Stern, 2004; Londin et al., 2005; Sasai et al., 1995), it is necessary for placode precursor formation at gastrulation, but must be switched off thereafter (Ahrens & Schlosser, 2005; Kwon et al., 2010; Litsiou et al., 2005). Likewise, neural crest cells need BMP activity early, but unlike placodes continue to do so as they are specified (Barth et al., 1999; Kwon et al., 2010; Liem et al., 1995; Marchant et al., 1998; Steventon et al., 2009). Finally, Wnt activity is required for neural crest cell induction (Garcia-Castro et al., 2002; Steventon et al., 2009) but must be inhibited for neural and placode precursors to form (Heeg-Truesdell & LaBonne,

2006; Litsiou et al., 2005; Patthey et al., 2008). These signals activate different transcription factor networks in a temporally and spatially controlled manner, which in turn are thought to impart cell identity and have therefore been termed fate 'specifiers'. For example, *Msx1* and *Pax3* have been implicated as NPB specifiers (Milet et al., 2013; Monsoro-Burq, 2015; Plouhinec et al., 2014), while *Pax7* (Basch et al., 2006) and *Six1* (Brugmann et al., 2004; Chen et al., 2009; Christophorou et al., 2009; Ozaki et al., 2004) are involved in neural crest and placode precursor specification, respectively. These factors appear to act in feed forward loops, upregulating their own expression while simultaneously repressing factors that specify alternative fates (for review: Grocott et al., 2012; Thiery et al., 2020).

Based on these studies combined with tissue transplantation experiments, two apparently contradictory models for the segregation of neural, neural crest and placodal fates have emerged (for review: Schlosser, 2006, 2014; Thiery et al., 2020). The 'binary competence model' suggests that an initial step in lineage segregation entails a subdivision of the ectoderm into neural/neural crest and placode/epidermal territories (Ahrens & Schlosser, 2005; Pieper et al., 2012; Schlosser, 2014). This implies a closer relationship of neural crest cells with the central nervous system and of placodes with the epidermis. In contrast, the 'NPB model' suggests that cells at the border of the neural plate have mixed identity and retain the ability to generate all ectodermal derivatives until after neurulation begins (Baker & Bronner-Fraser, 1997b; Roellig et al., 2017; Streit & Stern, 1999). Studies in *Xenopus* have taken this idea a step further, revealing that unlike other ectodermal cells, cells at the NPB retain pluripotency markers which is key for their multipotency (Buitrago-Delgado et al., 2015; Prasad et al., 2012). In support of this idea, the NPB region is initially characterised by co-expression of neural and non-neural markers (for review: Grocott et al., 2012; Pla & Monsoro-Burq, 2018; Thiery et al., 2020). Fate specifier genes are activated within this territory in partially overlapping patterns and resolve into distinct domains as neurulation begins. While both models are attractive and provide working hypotheses, the underlying experiments were analysed at cell population, rather than at single cell level. They therefore do not address how individual cells at the NBP make decisions, nor whether they are multipotent or a population of mixed progenitors that are already biased towards their later identity. Recent findings have proposed that prior to fate commitment, cells show increasing levels of heterogeneity in gene expression and do not exhibit a definitive transcriptional signature (Soldatov et al., 2019). It is therefore possible that cells at the NPB include such undetermined progenitor cells.

Studies in chick have begun to characterise cell heterogeneity at the NPB at a single cell level revealing that factors previously thought to be fate-specific are co-expressed in individual cells even at late neural tube stages (Roellig et al., 2017; Williams et al., 2022). Furthermore,

109 lineage tracing using a 'neural-specific' Sox2 enhancer shows that Sox2$^+$ cells can contribute
110 not only to neural tissue but also to neural crest and epidermis (Roellig et al., 2017). However,
111 these studies only surveyed a relatively small number of ectodermal cells and, focusing on
112 neural crest cells, did not include data for definitive placodal cells. It is therefore challenging
113 to assess how these fates segregate. Nevertheless, these findings suggest that cell fate
114 allocation at the NPB occurs over a much longer developmental period than previously thought
115 and that NPB cells retain plasticity until early neurulation. However, the underlying molecular
116 mechanisms of how individual cells make decisions at the NBP remain poorly understood.
117
118 Here, we explored the transcriptional changes as cells transit from the neural plate border at
119 early primitive streak to definitive neural, neural crest and placodal fates at single cell level (for
120 analysis workflow see Figure 1). In total we present single cell RNAseq (scRNAseq) data for
121 17,992 high quality cells. Rather than using 2-3 molecular markers to assign cell identity, we
122 established a binary knowledge matrix using previously published *in situ* hybridisation
123 expression data. This allows us to classify cells at each developmental stage, despite the high
124 levels of heterogeneity observed. We find that prior to head fold stages cells do not fall into
125 transcriptional distinct groups but are characterised by graded and partially overlapping gene
126 expression. An early cell population located at the NPB (eNPB) can be identified by co-
127 expression of neural and non-neural genes prior to the upregulation of fate specifiers. As
128 development proceeds, ectodermal cell diversity increases, with a division of neural and non-
129 neural fates becoming apparent at the first somite stage together with the emergence of neural
130 crest cells. By the 8-somite stage, neural, neural crest and placodal cells are largely
131 segregated, although even at this late stage we find cells with heterogenous expression
132 profiles.
133
134 Using a gene module approach, we identify dynamic changes in groups of genes that are
135 characteristic for neural, neural crest and placodal fates. Comparing co-expression of whole
136 gene modules (rather than individual transcripts) reveals that many cells at the NPB co-
137 express gene modules which later become restricted to placodal or neural crest lineages.
138 These cells may have the potential to give rise to both (or more) fates and we therefore refer
139 to them as 'Border-Located Unstable Progenitors' (BLUPs). Interestingly, as progenitors
140 segregate into their respective fates, we no longer identify NPB clusters but continue to find
141 BLUPs. BLUPs connect segregating cell populations, resembling previously characterised
142 bridge cells in the differentiating murine neural crest which exhibit high heterogeneity prior to
143 segregation (Soldatov et al., 2019). Here, we propose that BLUPs continue to be plastic until
144 neural tube closure, maintaining the ability to contribute to different fates. Overall, our analysis
145 highlights that although the NPB demarcates an anatomical region, it is not a discrete

146 transcriptional state. Instead, we identify BLUPs which we predict to be in an undetermined
147 state and to retain the potential to contribute towards alternative ectodermal fates.
148
149 **Results**
150
151 **Classification of ectodermal cells using a binary knowledge matrix of known marker**
152 **genes**
153
154 Neural, neural crest and placode cells arise from the embryonic ectoderm. However, how
155 individual progenitors acquire their terminal fates and the sequence and timing of their
156 segregation remain to be elucidated. To capture cells during this process, we carried out 10x
157 Genomics single-cell mRNA sequencing (scRNAseq) on cells taken from a broad region of
158 the chick epiblast at six developmental stages: HH4^{-}/4 (primitive streak), HH5 (head process),
159 HH6 (head fold), HH7 (1 somite), somite stage (ss) 4 and ss8 (Figure 2A). These stages were
160 chosen because they encompass the initial formation of the neural plate to the beginning of
161 neurulation when these fate decisions are thought to take place. After integration across
162 batches, stringent quality control and removal of contaminating cell populations (see methods
163 and Figure 2–figure supplement 1A-I), we captured a total of 17,992 high quality cells with
164 approximately 2500-4000 cells per stage and an average of 3924 genes per cell.
165 Dimensionality reduction and UMAP embedding reveals that cells at later stages displayed
166 higher cell diversity compared with earlier stages where most cells were transcriptionally
167 similar (Figure 2B-E and Figure 3A-D).
168
169 Typically, scRNAseq cell states are classified using a small number of definitive marker genes
170 which exhibit mutually exclusive expression patterns. However, this approach is difficult to
171 apply to the NPB for several reasons. Firstly, the early NPB cannot be classified using
172 definitive markers as it emerges in the region of overlap between neural and non-neural genes.
173 Secondly, cells at the NPB are thought to be in a transitory state before they acquire their
174 definitive ectodermal fate (neural, neural crest, placodal and epidermal). Finally, cells at the
175 NPB appear to be highly heterogeneous, with precursors for the different fates found
176 intermingled, even at late stages of neurulation (Bhattacharyya et al., 2004; Roellig et al.,
177 2017; Streit, 2002; Williams et al., 2022). To overcome these challenges, we categorised cells
178 using a binary knowledge matrix based on expression data obtained from the literature
179 (Supplementary File 1). We examined available *in situ* hybridisation data of 76 genes with
180 known regionalised expression patterns and binarized their expression within each defined
181 cell state. This allowed us to define a total of 24 cell states spanning primitive streak to neural
182 tube stages. Using this approach, we classify NPB cells not only by the expression of NPB

183 specifiers *Pax7* and *Tfap2a*, but also by the overlapping expression of early neural and non-
184 neural genes.
185
186 We first unbiasedly clustered cells from each developmental stage at a high resolution to
187 ensure capturing the full diversity of cell states (Figure 2–figure supplement 1J). Clusters were
188 then classified based on the similarity between their gene expression and the knowledge
189 matrix (see methods). This classification approach successfully identified 22 distinct cell states
190 within the ectoderm across all developmental stages. Early NPB and early neural cell
191 populations can already be identified at primitive streak stages, while placode progenitor and
192 neural crest states emerge at head process and ss4, respectively (Figure 2B and Figure 3A-
193 B).
194
195 **Cell states emerging from primitive streak to head fold stages**
196
197 To explore the temporal changes in cell diversity within the embryonic ectoderm, we compared
198 cell states present at different stages and identified the time point when each emerged. We
199 first examined stages HH4-HH6 to characterise events as the neural plate is established and
200 placodal and neural crest cells are thought to be specified.
201
202 *An early NPB population is identified at primitive streak stages prior to the expression of fate*
203 *specifiers*
204 By primitive streak stage, mediolateral (M-L) gradients of molecular markers demarcate pre-
205 neural and non-neural territories within the chick epiblast (Pera et al., 1999; Rex et al., 1997;
206 Sheng & Stern, 1999; Streit et al., 2000; Streit et al., 1998). At HH4, unbiased clustering clearly
207 organises cells in a pattern reminiscent of this M-L axis (Figure 2B; from left to right) as
208 evidenced by the expression of node (*ADMP*), pre-neural (*Yeats4, Sox3, Sox11*) and non-
209 neural (*Dlx5/6*, *Bmp4, Msx1, Tfap2a*) genes (Figure 2E and Figure 2–figure supplement 2A).
210 Cell states can be broadly characterised based on combinatorial gene expression (Figure 2E)
211 and we identify five cell states: node, early neural (eN), early neural plate border (eNPB), non-
212 neural ectoderm (NNE) and extraembryonic ectoderm (EE) (Figure 2B). While some genes
213 are shared between many cells, early neural plate cells are defined by high levels of pre-neural
214 transcripts while the non-neural and extraembryonic ectoderm are characterised by increased
215 non-neural gene expression. Notably, we identify that an early NPB population which co-
216 expresses both neural and non-neural genes. Thus, early NPB cells are already apparent prior
217 to the differential upregulation of genes previously characterised as NPB specifiers (*Msx1,*
218 *Pax7, Tfap2a, Dlx5/6, Pax3*) (Basch et al., 2006; Ezin et al., 2009; Hong & Saint-Jeannet,

219 2007; McLarren et al., 2003; Rothstein & Simoes-Costa, 2020; Streit & Stern, 1999) (for
220 review: Simoes-Costa & Bronner, 2015; Thiery et al., 2020).
221
222 *The first emerging NPB and PPR cells have regional identity*
223 At HH5, cell positions in the UMAP continue to reflect organisation along the M-L axis in the
224 embryo (Figure 2C), but new transcriptional states emerge. Whilst non-neural ectoderm cells
225 display a similar expression profile at HH5 compared to HH4, neural plate cells differ from
226 early neural cells in their expression of definitive neural (e.g., *Sox2*) and regional markers
227 (Figure 2E; Figure 2–figure supplement 2B). Like at HH4, many cells continue to co-express
228 neural and non-neural transcripts (Figure 2–figure supplement 2B). Within the latter cell group,
229 we observe the upregulation of PPR genes (*Six1*, *Eya2*; Figure 2C, E: aPPR, anterior PPR)
230 and for the first time NPB specifiers (*Msx1*, *Pax3, Pax7*; Figure 2C, E: pNPB, posterior NPB).
231 These observations correlate well with gene expression in the embryo. *Msx1* is initially
232 expressed in the extraembryonic and non-neural ectoderm, and together with *Pax7* begins to
233 be upregulated at the NPB thereafter (Basch et al., 2006; Streit & Stern, 1999), while PPR
234 markers are first expressed at HH5. Notably, the NPB initially has a posterior character, while
235 placode precursors have anterior identity based on their expression of *Gbx2* and *Six3*,
236 respectively (Figure 2E; see also below).
237
238 *Anteroposterior organisation of cells at head process and head fold stages*
239 Cells with distinct anteroposterior (A-P) character are first observed at HH5 through the
240 restricted expression of various homeobox transcription factors. *Rax* and *HoxB1* are highly
241 confined to distinct cell groups, whilst in contrast *Six3* and *Gbx2* exhibit broader negatively
242 correlated expression gradients across cell clusters with some degree of overlap (Figure 2E
243 and Figure 2–figure supplement 2B). The organisation of cells within the UMAP reflects the A-
244 P expression gradients of these genes in the embryo (Chapman et al., 2002; Hidalgo-Sanchez
245 et al., 2005; Ohuchi et al., 1999; Paxton et al., 2010). The overlap of A-P factors was used to
246 distinguish different NP, PPR and NPB regions during unbiased cell state classification
247 (Supplementary File 1).
248
249 Within the NP we can distinguish intermediate neural plate (iNP) states from the anterior and
250 posterior neural plate (aNP, pNP) and from early caudal neural (eCN) states. However, within
251 the PPR and NPB we identify only anterior (aPPR; *Six3*$^{+}$) and posterior (pNPB; *Gbx2*+) cell
252 states, respectively. While in UMAPs, aPPR cells are located between the NNE and anterior
253 NP, the pNBP cluster resides between the iNP and pPPR clusters (Figure 2C, E Figure 2–
254 figure supplement 2C), reflective of both its A-P and M-L position *in vivo*.
255

256 Between HH5 and HH6, posterior *Gbx2*$^{+}$ PPR (pPPR) cell states emerge (Figure 2D), as do
257 PPR cells that appear to lack regional identity. At this stage, *Otx2* and *Gbx2* expression
258 domains in the embryo abut (Steventon et al., 2012), suggesting that cells with generic PPR
259 character might be intermingled with those already biased towards axial identity and either
260 retain the potential to contribute to multiple axial levels or will later become intermediate PPR
261 cells.
262
263 Together, our data show that the emergence of cells with divergent transcriptional profiles
264 resembles patterning of the ectoderm *in vivo*. However, unbiased cell clustering forces cells
265 into discrete clusters which may not fully reflect heterogeneity in gene expression and cell
266 diversity. Indeed, our single cell data reveal the heterogenous nature of gene expression:
267 markers are broadly expressed and are not confined by cluster boundaries or by neighbouring
268 expression domains (Figure 2F-J, Figure 2–figure supplement 2C). Despite this heterogeneity,
269 our cell classification approach successfully identifies increased ectodermal cell diversity over
270 time, with neural, posterior NPB and anterior PPR cells emerging when the definitive neural
271 plate forms. Importantly, the relative positions of these cell states in the UMAPs reflect their
272 location in the embryo.
273
274 **Increasing cell diversity from 1-somite to 8-somite stages**
275
276 At HH7, the neural folds begin to elevate indicating the start of neurulation, while during early
277 somitogenesis neural crest cells start to migrate and placode precursors begin to diversify.
278 We therefore sought to characterise the transcriptional changes at single cell level as neural,
279 neural crest and placodal fates emerge.
280
281 Following clustering, we identified two major superclusters at HH7, one containing neural tube
282 and neural crest and the other placodal and future epidermal clusters (Figure 3A). These
283 superclusters appear to be largely separate, both by their UMAP embedding and the restricted
284 expression of definitive fate markers (Figure 3A, D). Whereas at earlier stages many cells co-
285 express non-neural and neural markers (Figure 2E, F, J), at HH7 cells expressing non-
286 neural/placodal (*Dlx5/6*, *Six1*) and neural transcripts (*Sox21*, *Sox2*) are largely confined to
287 their respective supercluster (Figure 3–figure supplement 1A). It is at this stage that anterior
288 NPB cells can first be identified transcriptionally, and together with posterior NPB cells they
289 connect the two superclusters (Figure 3A; aNPB, pNPB).
290
291 *The neural crest begins to be specified at early neurulation*

292 Adjacent to the NPB clusters, we observe a neural crest cell cluster expressing early definitive
293 neural crest markers including *Tfap2b*, *Snai2* and *Axud1* (*Csrnp1*) alongside NPB markers
294 (*Msx1*, *Pax7* and *Tfap2a*) (Figure 3D; NC and Figure 3–figure supplement 1A). Thus, neural
295 crest cells first emerge as a distinct cell population at HH7. Although many genes are shared
296 between the NPB and neural crest cell clusters, NPB cells also express PPR and non-neural
297 markers (*Six1*, *Eya2* and *Dlx5/6*) which are in turn downregulated in neural crest cells (Figure
298 3D and Figure 3–figure supplement 1A). Furthermore, we find that *Msx1* and *Pax7* are not
299 strongly expressed within placodal cell clusters. It is therefore possible that these markers do
300 not represent NPB specifiers, but rather an early bias towards neural crest fate.
301
302 *Neural, placodal and neural crest lineages are largely segregated by ss4*
303 At ss4 and ss8, a NPB cell cluster can no longer be identified using the above criteria. Instead,
304 we observe an increasing diversity of cells classified as placodal, neural crest or neural (Figure
305 3B, C, E). Within the neural cell population, forebrain, midbrain, and hindbrain (FB, MB, HB)
306 clusters are clearly distinguishable. *Six3* and *Gbx2* expression define cells with fore- and
307 hindbrain identity, respectively, whilst the upregulation of the dorsal midbrain marker *Wnt4*
308 *(Hollyday et al., 1995)* and mid/hindbrain boundary marker *Pax2* (Hidalgo-Sanchez et al.,
309 1999) highlights midbrain-like cells (Figure 3D and Figure 3–figure supplement 1B, C). As
310 development progresses, neural, neural crest and placode cells become increasingly distinct,
311 with neural crest cells beginning to express a suite of definitive neural crest markers, including
312 *Sox10* in the delaminating neural crest (dNC) cluster (Figure 3D).
313
314 Despite the apparent segregation of neural, neural crest and placodal fates at ss4 and ss8,
315 small cell populations connect PPR, neural crest, forebrain and midbrain clusters, in a four-
316 way pattern reflecting their A-P and M-L segregation *in vivo* (Figure 3B, C). To predict the
317 directionality of transcriptional change within these populations, and hence their potential
318 developmental trajectory, we performed RNA velocity analysis (Bergen et al., 2020; La Manno
319 et al., 2018). This analysis predicts that they move away from cluster boundaries, towards
320 definitive cell states (Figure 3F, G).
321
322 Together our data show that whereas cell states at HH4-HH6 exhibit broad overlapping gene
323 expression, definitive fate markers are upregulated from HH5 onwards and subsequently gene
324 expression is refined at the boundaries between cell clusters. At HH7 and ss4, placodal, neural
325 crest and neural fates begin to segregate. However, even as the neural tube closes, cells
326 continue to straddle cluster boundaries; these cells may be transcriptionally unstable and
327 therefore still actively undergoing fate decision processes.
328

Figure 3. Increased cell diversity and lineage segregation from HH7 to ss8. (A-C) UMAP plots for cells collected at HH7 (1 somite stage), ss4 (4 somite stage) and ss8 (8 somite stage). Cell clusters are coloured and labelled based on their semi-unbiased cell state classifications (binary knowledge matrix available in Supplementary File 1). **(D)** Dot plots displaying the average expression of key marker genes across cell states at HH7, ss4 and ss8. The size of the dots represents the number of cells expressing a given gene within each cell population. **(E)** Feature plots depicting the lineage restricted expression of neural (*Sox21*), placodal (*Six1, Dlx5, Tfap2a*) and neural crest (*Pax7, Tfap2a, Tfap2b*) markers. **(F-G)** UMAP plots for ss4 and ss8 overlaid with RNA velocity vectors depicting the predicted directionality of transcriptional change. Cells are coloured by cell state classification (shown in B and C). Schematics summarise the key fate segregation events taking place at these stages predicted by RNA velocity analysis.

Dynamic changes in gene module expression over time

Many transcriptional regulators and their interactions have been implicated in cell fate decisions as the ectoderm is specified and differentiates into its derivatives. However, studies have largely taken a gene candidate approach. To explore the full transcriptional dynamics of both known and new transcriptional regulators during the specification of neural, neural crest and placodal cells, we modelled the dynamics of whole gene modules rather than individual candidate genes. This allows us to investigate transcriptional dynamics in an unbiased manner whilst simultaneously minimising the loss of potentially important factors.

Defining neural, neural crest and placodal gene modules

To investigate the segregation of neural, neural crest and placode fates, we grouped together cells from all developmental stages (Figure 4A, B) and sought to identify gene modules that characterise each cell lineage. Gene modules are groups of genes that display similar expression profiles across a dataset. We calculated gene modules using the Antler R package (Delile et al., 2019), which iteratively clusters genes hierarchically based on their gene-gene Spearman correlation. This approach reveals 40 modules each showing highly correlated gene expression across all stages (HH4-ss8). To focus on gene modules which may include candidates for fate segregation, we included only those that are differentially expressed between any cell state and the rest of the dataset, and then filtered to remove those with differential expression between sequencing batches. Finally, since our data show that the segregation of neural, neural crest and placodal cell states is almost complete at ss8 (Figure 3C), we kept those gene modules that show differential expression between at least one of the three fates at ss8 (see methods). This resulted in nine modules that were considered further (Figure 4–figure supplement 1A and Figure 4–Source Data 1). Of these, four gene modules (GM21-24) are specifically expressed in the PPR at ss8, one (GM13) in neural crest

370 cells, and the remaining four (GM7, 9, 11, 20) are upregulated primarily in neural clusters
371 (Figure 4–figure supplement 1A).
372
373 When examining the genes within each module, we noticed that GM20 and GM22 include
374 genes with widespread expression or expression in the lateral mesoderm and/or the
375 extraembryonic region (*Epas1, Nkx2-5, Tnnc1, Pgk1*) (Adams et al., 2008; Bell et al., 2004;
376 Liberatore et al., 2000; Ota et al., 2007) (Figure 4–Source Data 1). We therefore removed
377 these modules from subsequent analysis. GM7 contains well characterised anterior markers
378 including *Otx2*, *Six3* and *Pax6*, whilst GM11 contains midbrain/hindbrain markers including
379 *Pax2*, *Nkx6-2* and *Wnt4* (Figure 4–Source Data 1). We find that at ss4 and ss8 these gene
380 modules are indeed upregulated in the forebrain/aPPR and midbrain/hindbrain, respectively
381 (Figure 4–figure supplement 1A). To focus our analysis on the segregation of neural, neural
382 crest and placodal cells rather than on A-P patterning, A-P restricted modules were removed.
383 The remaining five modules show broadly pan-neural (GM9), pan-placodal (GM21, GM23,
384 GM24) or neural crest cell (GM13) expression at ss4 and ss8 (Figure 4E).
385
386 *Latent time analysis suggests late emergence of neural crest cells*
387 Given the cellular heterogeneity observed at early timepoints, discrete developmental stages
388 do not necessarily accurately represent the developmental progression of individual cells
389 towards a given fate. In contrast, latent time can measure the biological clock of individual
390 cells as they differentiate and thus represents the order of cells along a developmental
391 trajectory. To explore the expression dynamics of the five selected gene modules as neural,
392 neural crest and placodal fates emerge, we first ordered cells across latent time using scVelo
393 for the entire dataset (Figure 4C and Figure 4–figure supplement 1B). To investigate the
394 segregation of all three fates, three separate trajectories need to be distinguished. To do this
395 we calculated the probability of each cell to transit towards one of three terminal states (Figure
396 4–figure supplement 1C). These probabilities were obtained using CellRank (Lange et al.,
397 2022), which leverages RNA velocity and transcriptomic similarity information to predict
398 transitions between cells. Visualising the fate probabilities across the full dataset shows that
399 cells with low latent time values (i.e., early cells) have low probabilities of becoming neural,
400 neural crest or placodal cells (Figure 4D, see Figure 4A for stage reference). As cells 'age' the
401 fate probability increases as they become transcriptionally similar to the terminal state. Unlike
402 placodal and neural fates, neural crest fate probabilities are only high in 'late' cells (Figure
403 4D), reflecting the fact that defined neural crest cell clusters only appear at HH7.
404
405 *Gene module dynamics reveals key differences in the activation of the transcriptional*
406 *programmes associated to neural, neural crest and PPR specification*

407 Having predicted the developmental trajectory of cells using scVelo and CellRank, we next
408 modelled the expression of the five selected gene modules as a function of latent time with
409 the aim to characterise their dynamics. Gene expression dynamics were modelled using
410 generalised additive models (GAMs). GAMs were chosen because gene expression is highly
411 dynamic and does not change linearly over time. For each gene module we fitted three
412 separate GAMs, one for each fate (Figure 4E; left). The three fates were distinguished using
413 the previously calculated fate absorption probabilities. This modelling approach reveals
414 dynamic changes of gene expression. Three gene modules – GM9, GM13, GM23 – are initially
415 inactive and are upregulated at different points across latent time in cells with neural, neural
416 crest and placodal character, respectively.
417
418 GM9 becomes upregulated in all neural clusters and includes neural markers like *Lmo1* and
419 *Sox21* (Figure 4E 'Neural GM9', Figure 4–Source Data 1). Although the expression of different
420 genes within this module correlates broadly, there is some gene-gene variation. For example,
421 *Lmo1* is the first gene to be expressed and exhibits highly dynamic expression over time. It is
422 first found at HH5 within the eCN, pNP and iNP, before being upregulated across the entire
423 neural plate at HH7 and ss4. At ss8, *Lmo1* is specifically downregulated within the MB. In
424 contrast, *Sox21* is first upregulated at HH5/6 and is consistently expressed throughout all
425 neural cell clusters.
426
427 In contrast, modelling reveals that GM13 is upregulated in cells with neural crest identity.
428 Indeed, it contains well known neural crest markers *Pax7*, *Snai2*, *Sox10* and *Tfap2b* (Figure
429 4E 'NC GM13', Figure 4–Source Data 1) and is initially broadly activated in NPB and neural
430 crest clusters at HH7. At ss4 and ss8, this module remains strongly expressed within neural
431 crest and delaminating neural crest clusters. Within GM13 individual genes are activated at
432 different time points: *Pax7* is the first gene to be expressed in the pNPB at HH5, while *Sox10*
433 starts to be expressed only from ss4 onwards.
434
435 Finally, modelling the expression dynamics of GM23 shows that it is activated early and
436 becomes upregulated in cells with placodal character across latent time. This prediction is
437 supported by the fact that GM23 is highly expressed in PPR clusters at ss8 and contains *bona*
438 *fide* placodal genes like *Six1* and *Eya2* (Figure 4E 'Placodal GM23', Figure 4–Source Data 1).
439 At HH4, most GM23 genes are not expressed, but are broadly activated at HH5 in PPR, non-
440 neural and NPB clusters, where they remain active until becoming restricted to PPR cells at
441 ss4. Comparing the onset of activation of these three gene modules across latent time reveals
442 a clear temporal order with the placodal module being activated first, followed by the neural
443 and neural crest gene modules.

In contrast to these modules, modelling of GM24 and GM21 shows that they are initially expressed in all three cell populations before being rapidly downregulated within neural crest and neural cells (Figure 4E 'Epiblast GM21' and 'Epiblast GM24'). Indeed, genes in GM24 are broadly expressed across the epiblast at HH4, and then become gradually restricted to PPR, non-neural and NPB clusters at HH6/7, and to PPR cells at ss4/8 (Figure 4A). GM21 displays similar dynamics but is restricted to non-neural clusters earlier at HH5. Although some genes within these epiblast modules have been described as non-neural/PPR specific based on *in situ* hybridisation (*Tfap2c*, *Bambi*, *Homer2*, *Tspan13*) (Bell et al., 2004; Hintze et al., 2017; Mehdizadeh et al., 2021; Reichert et al., 2013; Rothstein & Simoes-Costa, 2020), others are found to be expressed within the early neural territory (*Epcam*, *Sall4*, *Cited4*) (Barembaum & Bronner-Fraser, 2007; Bell et al., 2004; Trevers et al., 2021) (Figure 4–Source Data 1).

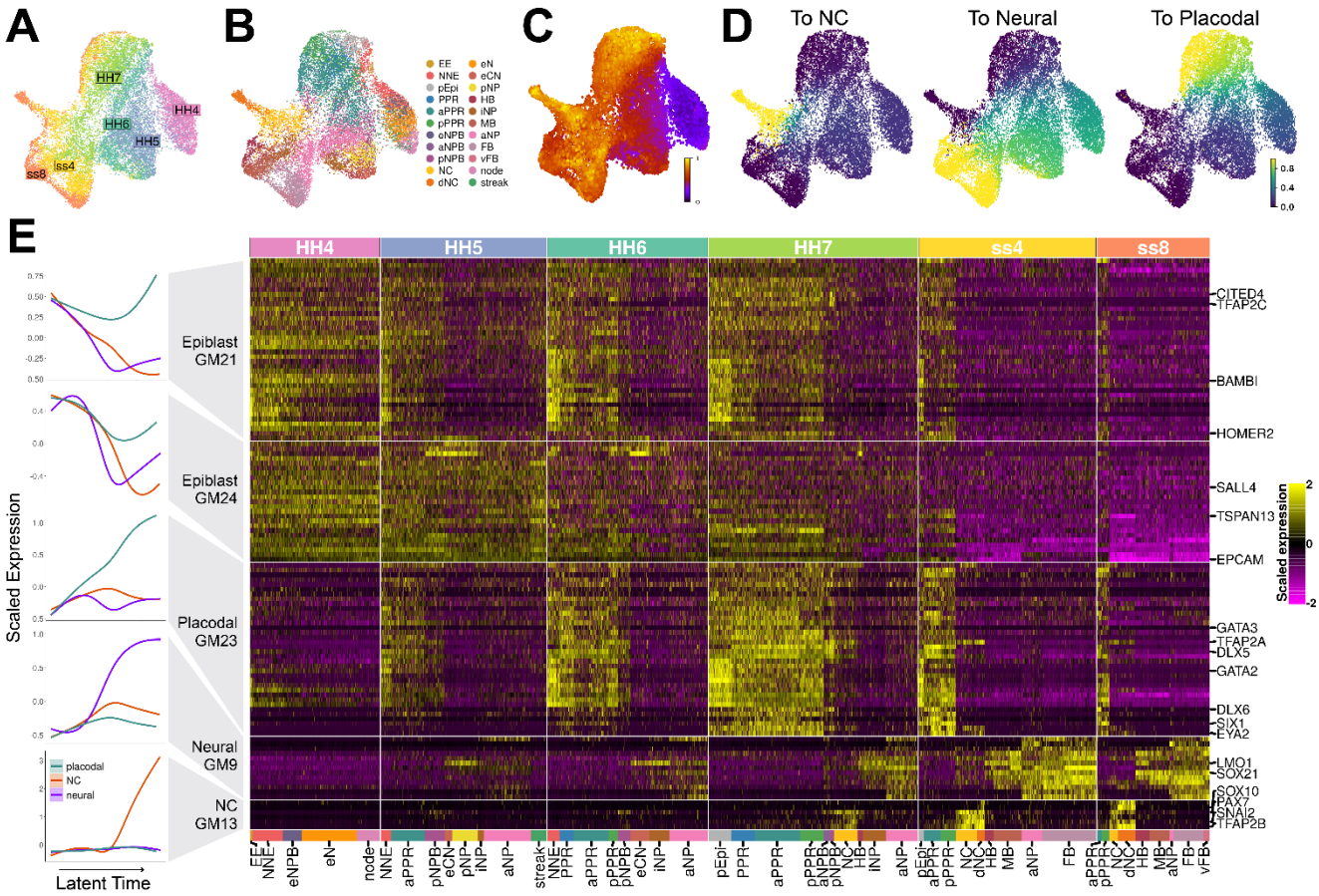

Figure 4. Gene module dynamics reveal key differences between the segregation of the PPR, neural crest and neural fates. (A) UMAP plot for the full dataset (HH4-ss8 combined) coloured and labelled by stage. **(B)** UMAP plot for the full dataset coloured by cell state classifications. Cell state classifications were calculated independently for each stage and transferred across for visualisation of the full dataset. **(C)** UMAP plot of the full dataset (HH4-ss8) showing cell latent time values. **(D)** UMAP plots of the full dataset showing the fate absorption probabilities of each cell towards one of the three defined terminal states: neural

465 crest, neural and placodal. **(E)** Left: Gene module dynamics plots displaying GAMs of scaled
466 gene module expression across latent time. GAMs are weighted by the fate absorption
467 probability of each cell towards one of the three terminal states (placodal, neural crest and
468 neural). Right: Heatmap of gene modules that display fate-specific expression (full list of gene
469 modules available in Figure 4-Source Data 1). Gene modules were first unbiasedly filtered
470 based on their differential expression between cell states (see methods and Figure 4-figure
471 supplement 1A). Gene modules were further manually filtered based on expression patterns
472 described in the literature (see results section: *Defining neural, neural crest and placodal gene*
473 *modules).* Key genes of interest are highlighted on the right (for full gene list see Figure 4-
474 Source Data 1).
475
476 In summary, modelling the expression dynamics of selected gene modules provides new
477 insight into the sequential activation of fate-specific developmental programmes, as well as
478 proposing key differences in the mechanism by which neural, neural crest and placodal cells
479 are specified. We show, using an unbiased gene module approach, that a placodal gene
480 module is activated first, followed by neural and neural crest modules. While neural and neural
481 crest modules are specifically activated in the relevant cell clusters alone, two modules that
482 are later restricted to the PPR are initially broadly expressed across the epiblast. We therefore
483 propose that the specification of neural and neural crest states may require the downregulation
484 of epiblast modules which later become confined to placodal cells.
485
486 **Spatially restricted co-expression of genes at the NPB**
487
488 Previously, the NPB has been defined based on the expression of so-called NPB specifiers,
489 however our transcriptome analysis suggests that these markers have either a placodal or
490 neural crest bias (Figure 3D). The question remains as to where NPB specifiers are co-
491 expressed; are they co-expressed throughout the border, or are putative unstable progenitors
492 spatially restricted? To investigate this, we sought to model the expression of 'NPB specifiers'
493 across the mediolateral axis, before validating their spatial expression *in vivo* using *in situ*
494 hybridisation chain reaction (HCR).
495
496 We chose to model the spatial expression of 'NPB specifiers' using our HH7 scRNAseq data
497 as this stage marks the start of placodal and neural crest segregation (Figure 3A). Principal
498 component analysis reveals that HH7 cells are ordered along the inverse of principal
499 component (PC) 1 based on their M-L position *in vivo*; PC1 therefore provides an axis through
500 which we can model spatial gene expression (Figure 5A). Smoothed expression profiles
501 across PC1 were modelled using GAMs calculated for each NPB specifier (Figure 5B).
502
503 Our models predict that *Msx1* and *Pax7* are upregulated medially relative to *Dlx6* and *Six1*, in
504 line with their roles in neural crest and placodal specification, respectively (Basch et al., 2006;

505 Brugmann et al., 2004; Christophorou et al., 2009; McLarren et al., 2003; Monsoro-Burq et al.,
506 2005). Interestingly, *Pax7* and *Six1*, which are upregulated later than either *Msx1* and *Dlx6*
507 (Figure 3E), are predicted to exhibit a smaller region of co-expression with each other than
508 with either *Msx1* or *Dlx6* (Figure 5C). This highlights that *Pax7* and *Six1* have a significant bias
509 towards either neural crest/placodal fates. *Tfap2a,* which is required for both placodal and
510 neural crest specification (Bhat et al., 2013; Rothstein & Simoes-Costa, 2020), is predicted to
511 overlap extensively with both *Pax7* and *Six1*.
512
513 HCR at the same stage validates the predicted levels of co-expression across the M-L axis *in*
514 *vivo* (Figure 5C-E). We quantified M-L expression by taking intensity measurements at three
515 different A-P positions (Figure 5C; yellow horizontal lines). The intensity measurements for
516 each gene were Z-scored across all three axial levels to allow for comparative relative
517 measurements of gene expression (Figure 5D). We note a striking correlation in the
518 expression intensity measurements taken from the intermediate axial level (Figure 5D;
519 Intermediate) and the predicted M-L expression patterns from our scRNAseq data (Figure 5B),
520 which represent an aggregate of all A-P regions.
521
522 Taken together, both our scRNAseq and HCR analysis reveal segregation of neural crest and
523 placodal markers across the M-L axis, with considerable heterogeneity in gene co-expression
524 depending upon the NPB markers in question. Importantly, there are striking differences of
525 gene expression and co-expression along the A-P axis. While *Dlx6* and *Six1* are strongly
526 expressed anteriorly, *Pax7* and *Msx1* show increased expression levels posteriorly (Figure
527 5D). Thus, cells within the anterior NPB may be biased towards placodal fates, whereas cells
528 located posteriorly may be biased towards neural crest cells. These findings suggest that only
529 a small subset of cells at the NPB are in an unstable state. Furthermore, while the NPB can
530 be defined as a territory adjacent to the developing neural plate, a unique NPB cell state
531 coinciding with this territory cannot be defined transcriptionally using previously established
532 criteria.

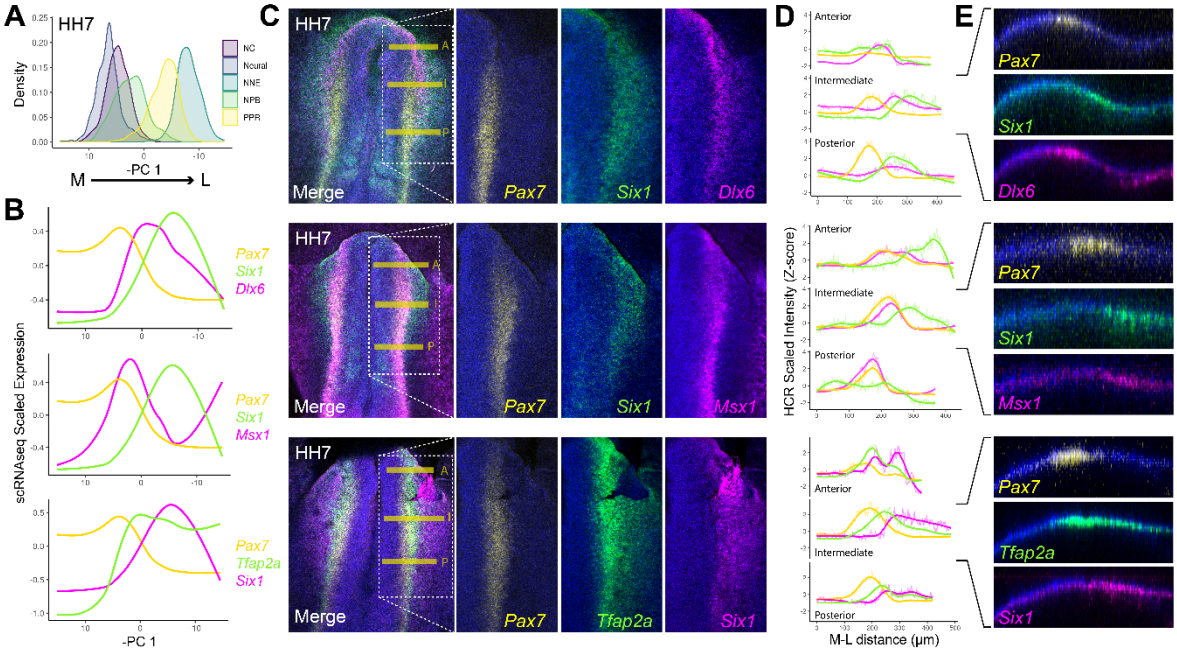

Figure 5. HCR validates spatial restriction of classical NPB specifiers. (A) Distribution of cells at HH7 from major ectodermal cell lineages across the inverse of principle component 1 (PC 1), revealing medio-lateral patterning across this axis. **(B)** Spatial gene expression modelling of key placodal and neural crest specifiers at HH7 across the inverse of PC 1. GAMs were fitted for each gene to predict their medio-lateral pattern of expression in the embryo. **(C)** Whole mount *in situ* HCR images at HH7 for combinations of markers modelled in B. Overlayed dotted boxes in the merged image show the region of interest displayed for each separated colour channel; yellow lines indicate the line where intensity measures in D were taken **(D)** Fluorescent intensity measurements taken at anterior 'A', intermediate 'I' and posterior 'P' regions depicted by the yellow bars in C. Intensity measurements were scaled for each gene across the three axial levels to allow for relative comparisons between different axial regions. **(E)** Virtual cross sections taken from the intermediate region, highlighting expression of each marker within the embryonic ectoderm.

BLUPs: multi-potent progenitors at the NPB?

Given the cell heterogeneity at the NPB, we sought to define an approach that did not depend on the expression of definitive NPB specifiers to identify and label transcriptionally unstable progenitors. Transcription factors that specify neural crest and placodal fates are known to cross-repress one another whilst enhancing their own expression (for review: Thiery et al., 2020). Therefore, cells that co-express placodal and neural crest genes may represent unstable progenitors which retain plasticity; we term these co-expressing cells 'Border-Located Unstable Progenitors' (BLUPs).

Defining neural crest and placode specific gene modules

559 To locate BLUPs within the ectoderm, we identified gene modules that are restricted to either
560 neural crest or placodal cells at late stages (ss8) and investigated their co-expression at earlier
561 stages. 15 modules were differentially expressed in at least one cell state (Figure 6–figure
562 supplement 1A and Figure 6–Source Data 1). GM9-13 and GM16-17 are characteristic for
563 neural cells with different A-P identities. Seven gene modules are absent from neural
564 populations but expressed in placodal cells (GM4-6), neural crest (GM1-2) or both (GM7-8).
565 GM5 contains well characterised placodal markers including *Six1*, *Homer2* and *Znf385c* and
566 is expressed in both aPPR and pPPR clusters. This module was therefore selected as a pan-
567 placodal module. GM2 is expressed in both neural crest and delaminating neural crest clusters
568 and contains neural crest specifiers like *FoxD3*, *Snai2*, *Sox9*, *Pax7* and *Msx1*, as well as the
569 Wnt ligands *Wnt1* and *Wnt6*. GM2 thus represents a *bona fide* neural crest specific module.
570 Although GM1 contains multiple neural crest markers (*Ets1*, *Sox10*, *Sox8*; Figure 6–Source
571 Data 1), it is only expressed in delaminating neural crest cells and was therefore excluded for
572 further analysis. Thus, GM5 and GM2 were considered as pan-placodal and pan-neural crest
573 module and used for co-expression analysis (Figure 6A).
574
575 *BLUPs co-express placodal and neural crest lineage specifiers*
576 To investigate the co-expression of these modules in NPB cells and their derivatives, we first
577 selected NPB (aNPB, pNPB), neural crest (NC, dNC) and PPR (aPPR, pPPR, PPR) cell
578 clusters from HH5-ss8 (Figure 6–figure supplement 1B, red cells; thereafter referred to as
579 NPB subset). Next, we re-clustered this subset of cells (Figure 5B). UMAP analysis highlights
580 a bifurcation of neural crest and placodal fates between HH7 and ss4, with the NPB located
581 at the boundary between neural crest and aPPR cell clusters (Figure 6B, C).
582
583 To examine the relative expression of pan-placodal and pan-neural crest modules within the
584 NPB subset, we ordered cells according to the expression ratio of both modules and grouped
585 them into 10 evenly sized bins (Figure 6D and Figure 6–figure supplement 2). Cells at the
586 extreme ends exclusively express the pan-neural crest (Bin 1) or the pan-placodal gene
587 module (Bin 10). As expected, these cells represent mostly delaminating neural crest or
588 placodal cells, respectively. However, cells in Bin 3 show equal expression levels of both
589 modules and contain a mixture of NPB, PPR and neural crest cells (Figure 6D). Mapping Bin
590 3 cells back to the UMAP revealed that BLUPs are located specifically between PPR and
591 neural crest cell clusters (Figure 6E).
592
593 To evaluate the distribution of BLUPs at different developmental timepoints, we mapped Bin
594 3 cells back to the UMAPs of individual stages (Figure 6–figure supplement 1C). We find at
595 HH5 and HH6, Bin 3 cells map to aPPR and pNPB clusters, whilst they map predominantly to

596 neural crest and NPB clusters at HH7. At ss4, there is a sharp reduction in the number of Bin
597 3 cells. Interestingly, although there is no cluster classified as NPB at this stage, BLUPs are
598 still located at the boundary between neural crest and PPR clusters and are predicted to be in
599 an undetermined transcriptional state by RNA velocity (Figure 3G). Once placodal and neural
600 crest fates are largely segregated at ss8, only very few scattered cells express similar levels
601 of pan-neural crest and pan-placodal modules.
602
603 The analysis above focuses on cells expressing similar levels of pan-placodal and pan-neural
604 crest modules. Next, we visualised cells that co-express these modules at different levels. We
605 calculated pan-neural crest and pan-placodal module co-expression per developmental stage
606 and filtered cells below a minimum heuristic threshold of 0.3 (Figure 6H). At HH5/6 almost all
607 cells classified as NPB and placodal cells co-express both modules above the threshold.
608 However, this changes at HH7, when co-expressing BLUPs are largely restricted to the NPB
609 and neural crest clusters. By ss4, only a small population of BLUPs found between placodal
610 and neural crest clusters continue to co-express alternative fate markers. Over time, we note
611 a striking shift in the distribution of co-expression between cells (Figure 6I). At early stages
612 (HH5-7) most cells co-express pan-placodal and pan-neural crest gene modules at similar
613 levels, whilst at later stages (ss4 and ss8) only a small subset of cells retain high relative levels
614 of co-expression (Figure 6I, boxes). This shift in distribution in the number of highly co-
615 expressing cells suggests that placodal/neural crest segregation takes place from around HH7
616 until ss8.
617
618 This analysis highlights that BLUPs are transcriptionally unstable, co-expressing gene
619 modules that characterise both neural crest and placodal cells. This expression profile is likely
620 to endow them with the potential to give rise to both, if not all NPB fates. The NPB demarcates
621 an anatomical region surrounding the neural plate, however it lacks a definitive transcriptional
622 signature highlighting that it is transcriptionally heterogeneous. Given the previously
623 characterised cross repressive interactions between placodal and neural crest specifiers (for
624 review: Thiery et al., 2020), we propose that unstable NPB progenitors (BLUPs) are better
625 defined based on the co-expression of alternate gene modules. The proportion of these cells
626 decreases over time, but a small population at ss4 retains this characteristic and is therefore
627 likely to retain bi- or multipotency even as the neural tube closes. We have shown that BLUPs
628 are likely in an unstable transcriptional state, however how this transcriptional heterogeneity
629 is resolved requires further exploration.
630
631
632

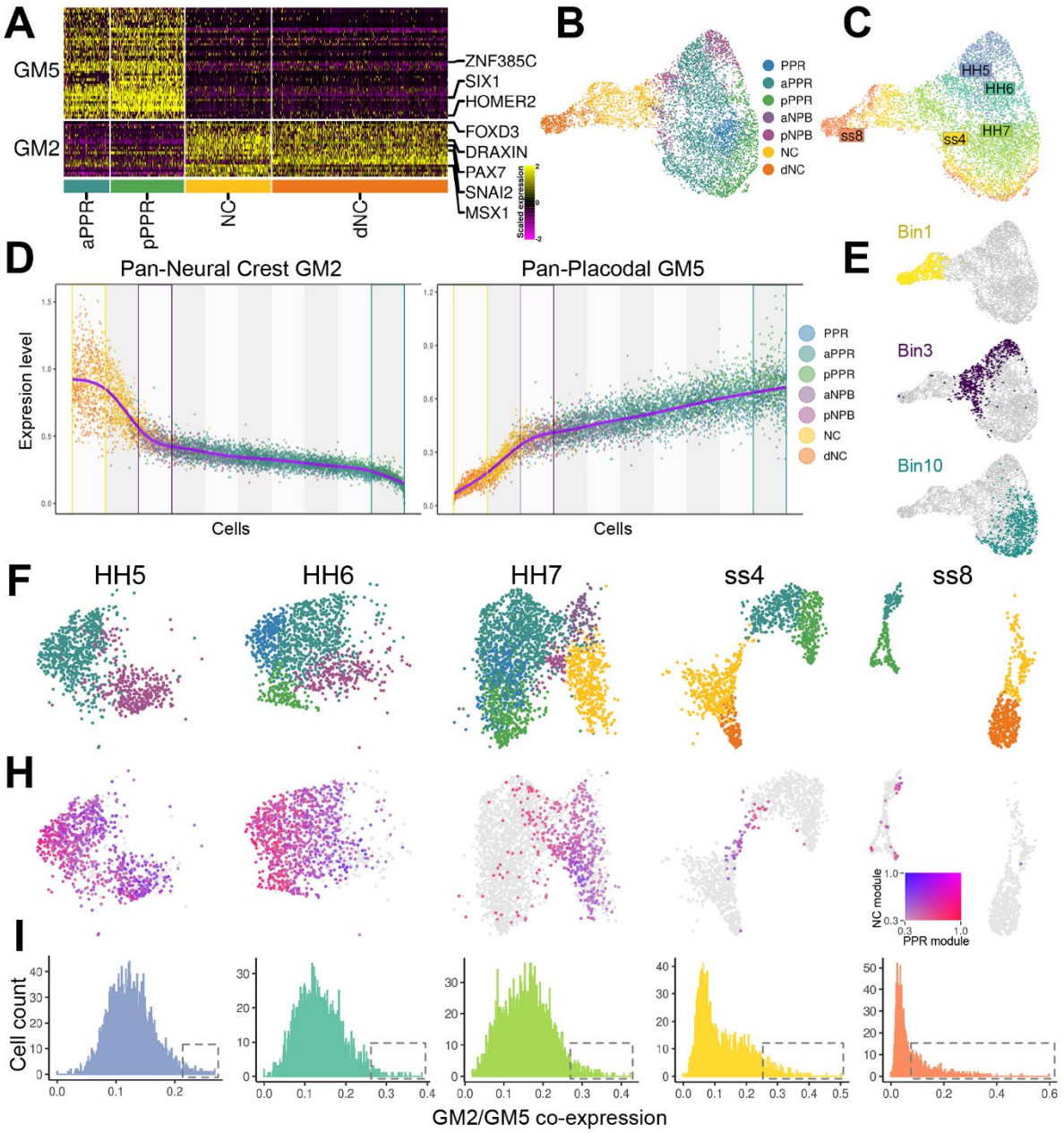

Figure 6. Border-Located Unstable Progenitors' (BLUPs) co-express placodal and neural crest gene modules. (A) Heatmap displaying pan-placodal (GM5) and pan-neural crest (GM2) at ss8 which have been subset from gene modules in Figure 6-figure supplement 1A. **(B)** UMAP plot of the NPB subset coloured by cell state. **(C)** UMAP plot of the NPB subset coloured by developmental stage. **(D)** Average normalized expression of placodal and neural crest gene modules (GM5 and GM2, respectively) identified at ss8 (see Figure 5). Cells are ordered by their expression ratio of these two modules and coloured by cell state. Cells were grouped into 10 evenly sized bins (background shaded regions). Three bins (1, 3 and 10) are overlaid to highlight cells with high neural crest/low placodal (bin 1), equivalent levels of both (bin 3) and high placodal/low neural crest (bin 10) gene expression. **(E)** UMAP plots of the NPB subset displaying the cells captured within bins 1, 3 and 10. **(F-H)** UMAP plots from each developmental stage, displaying only cells in the NPB subset (equivalent to red cells in Figure 6-figure supplement 1B). **(F)** Cells are coloured by cell state. **(H)** Co-expression analysis of the pan-neural crest and pan-placodal modules (see methods). Cells which co-express both

649 modules above 0.3 are coloured. **(I)** Histograms revealing the distribution of co-expression of
650 the pan-neural crest and pan-placodal modules at each developmental stage. At later stages
651 (ss4-ss8), the distribution of co-expression shifts from a normal to a negative binomial
652 distribution.
653
654
655 **Identifying a temporal gene expression hierarchy regulating the specification of neural**
656 **crest and placodal fates**
657
658 To investigate how BLUPs segregate towards neural crest and placodal fates, we modelled
659 gene module dynamics across the NPB subset (for workflow explanation see Figure 4–figure
660 supplement 2). We previously characterised gene expression dynamics (Figure 4E) across
661 the whole dataset and uncovered sequential activation of placodal, neural and neural crest
662 gene programmes. However, focusing on the NPB subset alone provides a higher resolution
663 of the gene expression hierarchy regulating the segregation of placodes and neural crest.
664
665 To model gene expression dynamics during lineage segregation at the NPB, we performed
666 scVelo analysis on the NPB subset (Figure 7A) and used CellRank to determine the probability
667 that each cell will become neural crest or placodal (Figure 7A-D). We then identified putative
668 lineage specifiers by calculating gene modules which are differentially expressed between
669 placodes and the neural crest. These 10 differentially expressed gene modules were further
670 filtered to include only those that contained genes expressed in neural crest, delaminating
671 neural crest or PPR cell states (as defined in the binary knowledge matrix). This analysis
672 identified three modules (GM12-14) upregulated in placodal and four in neural crest cells
673 (GM40 and GM42-44) between HH7 and ss8 (Figure 7E, Figure 7–Source Data 1). Using our
674 latent time and lineage probability measurements, we model the dynamics of these 7 gene
675 modules during the segregation of the placodes and neural crest (Figure 7E; left).
676
677 Of the placodal modules, GM14 and GM12 are expressed as early as HH5. GM12 is
678 expressed throughout both aPPR and pNPB and contains early non-neural/PPR markers like
679 *Gata2/3* (Figure 7E, Figure 7–Source Data 1). At HH6, GM12 is downregulated in the NPB
680 and remains confined to the PPR clusters until ss8. Unlike GM12, GM14 is initially restricted
681 to the PPR and only activated in the NPB at HH7. At ss4 and ss8 its expression is confined to
682 the PPR, with a higher expression in anterior cells. This module contains pan-placodal genes
683 *Dlx5/6* as well as anterior markers *Six3* and *Pax6*. GM13 is the last placodal module to be
684 activated and contains the definitive placodal transcripts *Six1* and *Eya2*. It is first expressed
685 at low levels at HH6 before being broadly activated across the PPR at HH7 through to ss8.
686 We also observe weaker expression of this module at the NPB cells at HH7. To visualise the

687 sequential activation of these modules across latent time, gene expression of each cell was
688 weighted based on its placodal fate probability. This analysis shows that GM12 is activated
689 before GM14 and GM13 in latent time. Whilst the expression of GM12 and GM14 does not
690 change dramatically, GM13 is highly upregulated over latent time within the placodal cells
691 (Figure 7E and Figure 7-figure supplement 1A).
692
693 The four neural crest gene modules each contain *bona fide* neural crest transcriptional
694 regulators including *Msx1*, *Zic1*, *Zeb2*, *Lmx1b* (GM40), *Pax7*, *Snai2*, *Axud1*, *Foxd3*, *Tfap2b*,
695 *Sox9* (GM42), *Sox5*, *Id1/2* (GM44) and *Sox10*, *Ets1*, *Lmo4* and *Sox8* (GM43) (Figure 7E and
696 Figure 7–Source Data 1). Our analysis groups these factors unbiasedly into four modules;
697 modelling their expression across latent time weighted by neural crest fate probability shows
698 a clear sequential activation from GM40 to GM42, GM44 and GM43 (Figure 7–figure
699 supplement 1). GM40 is activated first, initially broadly across aPPR and pNPB clusters at
700 HH5 and HH6, before becoming restricted to neural crest and NPB clusters from HH7
701 onwards. By ss8, it is downregulated in the delaminating neural crest population. GM42 and
702 GM44 are highly upregulated only in neural crest and delaminating neural crest cells, with
703 GM42 first expressed at HH7 and GM44 at ss4. Lastly, GM44 is activated specifically within
704 the delaminating neural crest cells at ss4 where it is further upregulated at ss8 (Figure 7E).
705 This order suggests a hierarchical relationship between these factors in the neural crest gene
706 regulatory network.
707
708 While gene module selection was based on prior knowledge of marker genes, this analysis
709 also allows us to predict novel factors with similar expression profiles. We selected *Ass1* and
710 *Olfml3* to validate the expression of novel placodal and neural crest markers, respectively,
711 using HCR (Figure 7F, G). Like the placodal specifiers *Six1* and *Eya1, Ass1* is found in GM13.
712 HCR confirms that *Ass1* and *Six1* are co-localised within the lateral NPB at HH7 and ss4, and
713 in the otic placode at HH11 (Figure 7G). However, we also note a greater degree in co-
714 expression of *Pax7/Ass1* than *Pax7/Six1* (Figure 7G; HH7 and ss4), as expected given our
715 gene expression dynamics predicts that *Ass1* is initially upregulated in both placodal and early
716 neural crest cells before it is downregulated in the neural crest (Figure 7H, I). *Olfml3* was
717 chosen as a novel neural crest marker, as it is found in GM44 which is predicted to be
718 upregulated within the neural crest in between GM42 (Pax7) and GM43 (*Sox10*) (Figure 7H).
719 HCR confirmed the predicted sequential temporal expression of these markers, with *Pax7*
720 active in the posterior NPB at HH7, *Pax7* and *Olfml3* co-expressed at NPB at ss4, and all three
721 markers expressed within the neural crest at HH11 when the neural crest is undergoing
722 delamination (Figure 7F).
723

In summary, analysing gene module dynamics across the NPB subset reveals the sequential activation of different co-regulated genes in placodal and neural crest cells. Many genes within these modules have been previously characterised and are known to form part of the neural crest or placode gene regulatory network (for review: Grocott et al., 2012; Pla & Monsoro-Burq, 2018; Schlosser, 2006, 2014; Simoes-Costa & Bronner, 2015; Thiery et al., 2020). This unbiased approach groups these factors and predicts a hierarchical order, as well as identifying new candidate factors which may play important roles in the segregation of the neural crest and placodal fates.

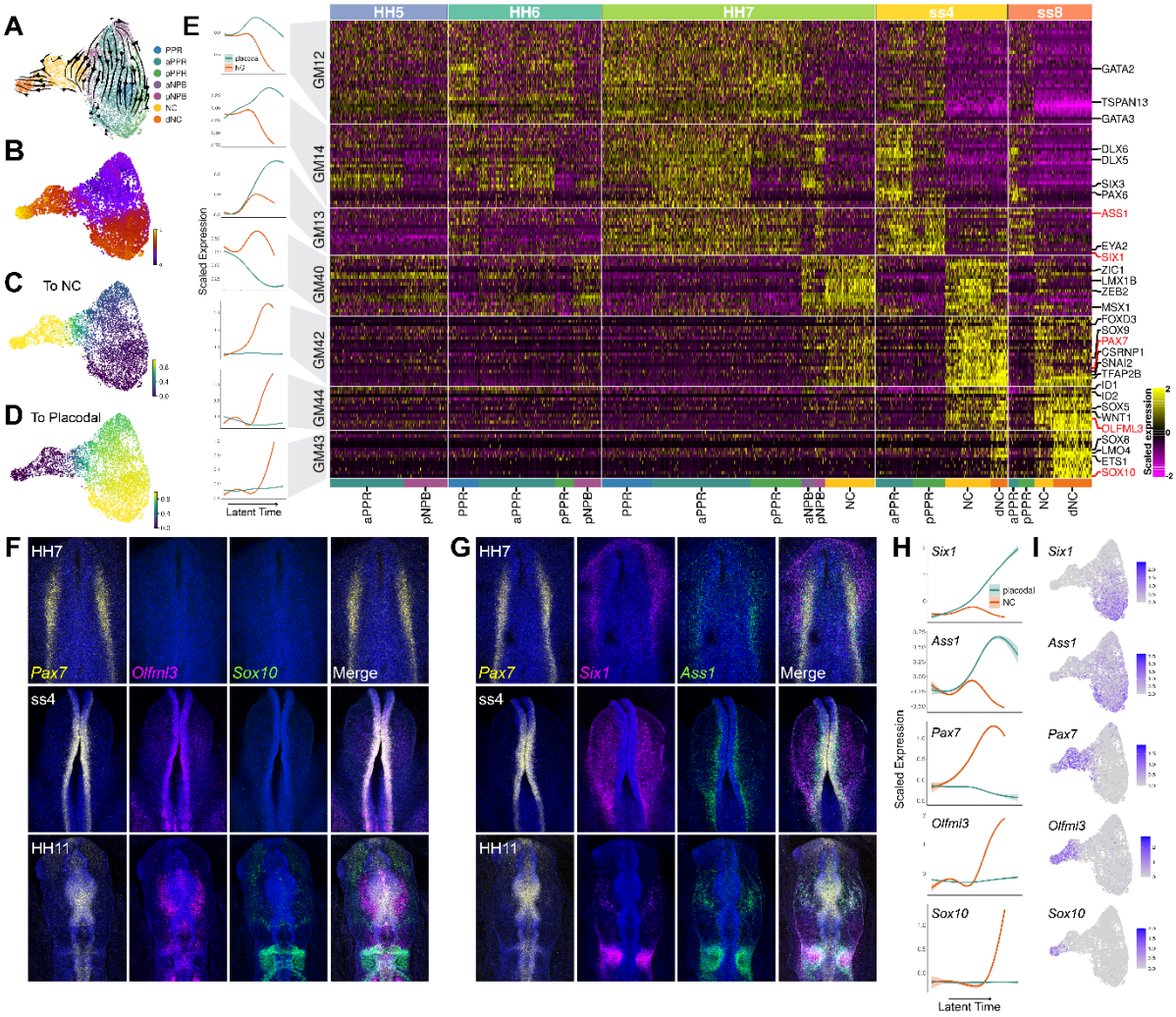

Figure 7. NPB gene module analysis reveals temporal hierarchy of gene expression during the specification of neural crest and placodes. (A) UMAP plot with cells coloured by cell state classifications and overlaid with RNA velocity vectors depicting the predicted directionality of transcriptional change. **(B)** UMAP plot of the NPB subset with cells coloured by latent time. **(C-D)** UMAP plots showing the fate absorption probabilities of each cell towards the specified terminal states (neural crest or placodes). **(E)** Left: Gene module dynamics plots displaying GAMs of scaled gene module expression across latent time. GAMs are weighted by the fate absorption probability of each cell towards either placodal or neural crest terminal states. Right: Heatmap showing gene modules calculated across the NPB subset (full list of

742 gene modules available in Figure 7-Source Data 1). To identify gene modules potentially
743 involved in placodal or neural crest specification, gene modules were filtered to include those
744 that show differential expression between placodal and neural crest cell states (see methods).
745 Genes specified as neural crest or placodal in our binary knowledge matrix (Supplementary
746 File 1) were selected as bait genes to further filter the gene module list for visualisation. Known
747 and novel placodal and neural crest markers highlighted in red were validated by *in situ* HCR
748 (F-G). **(F)** Whole mount *in situ* HCR at HH7, ss4 and HH11 validating the expression of *Olfml3*
749 at the NPB and delaminating neural crest. **(G)** Whole mount *in situ* HCR at HH7, ss4 and
750 HH11 validating the expression of *Ass1* in the pre-placodal region. **(H)** Gene dynamics
751 displaying GAMs of scaled gene expression across latent time. GAMs are weighted by the
752 fate absorption probability of each cell towards either placodal or neural crest lineages. **(I)**
753 Feature plots for genes validated by *in situ* HCR on the HH7 stage UMAP.
754

755 **Discussion**

756

757 The regulation of cell fate specification at the NPB has been extensively studied in a range of
758 model systems, giving rise to a wealth of knowledge regarding transcriptional regulators and
759 their interactions. Nevertheless, our understanding as to how individual cells undergo cell fate
760 decisions has been limited by our inability to study transcription and gene regulation at a single
761 cell level. Single cell immunohistochemistry has demonstrated that in contrast to what was
762 previously thought, cells co-express markers that specify either placodal, neural or neural crest
763 fates, even at late neurulation (Roellig et al., 2017). A recent single cell RNAseq analysis has
764 attempted to characterise transcriptional heterogeneity in the ectoderm, and proposed that a
765 definitive NPB is not established until early neurulation (HH7), at which point placodal and
766 neural crest lineages gradually segregate (Williams et al., 2022). However, an absence of
767 definitive placodal cells collected at late neurulation, as well as a low number of ectodermal
768 cells sampled limits the overall characterisation of ectodermal heterogeneity and makes
769 conclusions about placodal and neural crest segregation problematic. Nevertheless, newly
770 characterised cellular heterogeneity requires us to revisit models for cell fate specification at
771 the NPB and to reconsider our definition of the NPB itself.

772

773 In this study, we characterise ectodermal cell states and cellular heterogeneity from primitive
774 streak stages though to late neurulation in chick. We demonstrate that although significant
775 transcriptional differences are apparent between cells at primitive streak stages, due to high
776 levels of heterogeneity, cells do not cluster into discrete cell states exhibiting restricted
777 expression patterns until early neurulation (HH7). Instead, cell states are initially characterised
778 by the overlapping expression of broad early neural and non-neural genes, as well as axial
779 markers. We identify increased cell state diversification during neurulation, and segregation of
780 neural, neural crest and placodal lineages taking place across 1-somite to 8-somite stages.
781 High resolution transcriptional analysis of cells at the NPB reveals that by the 4-somite stage,
782 placodal and neural crest lineages have largely segregated. However, despite this

783 segregation, we continue to identify high levels of co-expression of placodal and neural crest
784 genes within BLUPs which are predicted to be in a dynamic transcriptional state.
785
786 *Specification of neural and neural crest cell lineages requires downregulation of broad epiblast*
787 *modules*
788
789 Although specification networks for the neural, neural crest and placodal lineages are well
790 established (for review: Betancur et al., 2010; Grocott et al., 2012; Pla & Monsoro-Burq, 2018;
791 Stundl et al., 2021; Thiery et al., 2020), the order in which these lineages are specified remains
792 unclear. Our unbiased gene module analysis has identified groups of genes which correlate
793 and are specifically upregulated within each cell fate. Our gene modules support the
794 specification networks established in previous studies. *Pax7*, *Tfap2b*, *Snai2* and *Sox10* cluster
795 together and are upregulated in neural crest states, while *Six1*, *Eya2*, *Gata2/3* and *Dlx5/6* are
796 activated within placodal states and *Lmo1* and *Sox21* in neural states.
797
798 We also find putative novel regulators of these cell states that are co-regulated with known
799 fate specifiers, as well as the order in which these cell fates are specified. Placodal, neural
800 and neural crest specific gene modules are activated sequentially, suggesting that these
801 states are specified in that order. However, there is also asynchrony in the initiation of cell
802 lineage specification; although we classify placodal cells as early as HH5, we also identify
803 transcriptionally unstable BLUPs at ss4. This suggests cell fate allocation at the NPB is a
804 gradual process, with the number of unspecified progenitors decreasing over time as they
805 commit to a given lineage.
806
807 Alongside characterising placodal, neural and neural crest gene modules, we observe the
808 expression of two modules which exhibit initial broad pan-epiblast expression at primitive
809 streak stages, but which are confined to placodal cell states at the 4 and 8-somite stages.
810 Within these epiblast modules, unsurprisingly we note the expression of important placodal
811 and non-neural genes *Tfap2c*, *Homer2* and the BMP inhibitor *Bambi*. In addition, we also find
812 the pluripotency marker *Sall4* and *Tspan13*, with the latter shown to be positively regulated by
813 Six1 (Mehdizadeh et al., 2021). A recent study in chick suggests that based on transcriptional
814 profiling a 'pre-border' state can already be defined prior to gastrulation. *In vitro* experiments
815 show that the pre-gastrula epiblast is specified as NPB; once cells have acquired a 'pre-border'
816 state they can become neural and placodal precursors depending on the signalling input
817 (Trevers et al., 2018). Given that the expression of epiblast modules becomes confined to the
818 placodes, we speculate that the specification of the neural crest and neural states might
819 require the downregulation of these modules.

820

821 *Identifying BLUPs at the neural plate border based on the co-expression of competing gene*
822 *modules*

823

824 Members of Zic, Tfap2, Pax, Msx and Dlx transcription factor families have previously been
825 termed NPB specifiers (for review: Stundl et al., 2021; Thiery et al., 2020). Tfap2a has been
826 identified as a pioneer factor which triggers the expression of other NPB specifiers and is
827 required but not sufficient for both neural crest and placodal cell fates (Bhat et al., 2013;
828 Rothstein & Simoes-Costa, 2020). The cell fate switching role of Tfap2a depends upon its
829 association with its co-factors, Tfap2b and Tfap2c. Tfap2c is necessary for the induction of
830 NPB specifiers *Msx1*, *Pax7* and *Zic1*, whilst Tfap2b is later required for downstream neural
831 crest specification (Rothstein & Simoes-Costa, 2020).

832

833 Gene module analysis across the neural plate border highlights the sequential activation and
834 restriction of previously characterised NPB specifiers to neural crest cells. Early NPB
835 specifiers *Msx1* and *Zic1* are initially broadly expressed across pNPB and aPPR cells at HH5,
836 but later become downregulated in placodal cells and upregulated in the neural crest. The
837 gene module containing *Pax7* is activated slightly later and contains other NPB specifiers
838 *Axud1* and *Tfap2b*, as well as definitive neural crest markers *FoxD3* and *Snai2*. Unlike the
839 *Msx1* module, which is initially upregulated in both aPPR and pNPB clusters at HH5, the *Pax7*
840 module is specifically restricted to the NPB and subsequent neural crest clusters (Figure 7E).
841 This analysis reveals that despite these markers having been previously characterised as NPB
842 specifiers, their expression becomes restricted to the neural crest. In contrast, *Dlx5/6* and
843 *Tfap2a* are both found within a gene module that is later restricted to the placodes (Figure 4E).

844

845 Although *Tfap2a* is grouped in the same module as placodal specifiers *Six1* and *Eya2*, it is
846 expressed in both placodal and neural crest cell states, even at later stages (Figure 3D, E).
847 This expression reflects the key role of *Tfap2a* as a pioneer factor in both neural crest and
848 placodal specification, however its expression alone is not sufficient to classify putative multi-
849 potent progenitors at the NPB. At HH5, although *Tfap2a* is expressed within the pNPB cluster
850 alongside other NPB specifiers, it is also expressed within aPPR cells which never express
851 NPB specifiers including *Pax7*, *Pax3* and *Tfap2b* (Figure 2E).

852

853 To classify the NPB as a discrete state, NPB markers need to be uniformly upregulated in
854 NPB cells which give rise to neural, non-neural ectoderm, neural crest and PPR fates. Given
855 the non-uniform expression of previously characterised NPB specifiers (Basch et al., 2006;
856 Ezin et al., 2009; Hong & Saint-Jeannet, 2007; McLarren et al., 2003; Rothstein & Simoes-

857 Costa, 2020; Streit & Stern, 1999), and the expression of *Tfap2a* in the early aPPR cells which
858 are unlikely to give rise to other fates, we propose that the NPB cannot be accurately classified
859 using just these previously established genes. Instead, the NPB is an anatomical region
860 surrounding the neural plate within which putative unstable progenitors (BLUPs) reside.
861 BLUPs can be identified through the co-expression of gene modules which regulate the
862 specification of alternative cell fates.
863
864 *Gradient border model resolves the neural plate border and binary competence dilemma*
865
866 The 'binary competence' and 'neural plate border' models have provided useful frameworks
867 for understanding cell fate determination during neural, neural crest and placodal segregation
868 (Figure 8A, B) (for review: Schlosser, 2006, 2014; Thiery et al., 2020). The binary competence
869 model suggests that the ectoderm is subdivided into non-neural/placodal and neural/neural
870 crest domains (Ahrens & Schlosser, 2005; Pieper et al., 2012), whilst the neural plate border
871 model suggests cells at the border remain multi-potent and can differentiate into all ectodermal
872 fates (Baker & Bronner-Fraser, 1997b; Roellig et al., 2017; Streit & Stern, 1999). Due to the
873 limitations of studying cell fate competence at a population level, transplantation experiments
874 have failed to resolve these two models.
875
876 Our co-expression analysis of pan-neural crest and pan-placodal gene modules revealed that
877 most cells in the early NPB can be classified as BLUPs, as they co-express these modules at
878 similar levels. At later stages, we see a divergence in the level of co-expression between cell
879 populations, with the highest co-expressing cells located at the branching points between the
880 neural crest and placodal lineages (Figure 6H and I). In summary, we find that over time, the
881 BLUP population reduces in size until it is restricted to only a small number of cells at the
882 boundary between placodal and neural crest cell clusters at the 4-somite stage. Cell fate
883 allocation within BLUPs is likely to be driven via transcription factor cross-repression, given
884 the previously characterised cross-repressive interactions taking place between placodal,
885 neural crest and neural specifiers (Brugmann et al., 2004; Christophorou et al., 2009;
886 Schlosser et al., 2008; Wakamatsu et al., 2004).
887
888 Following these findings, we propose a 'gradient border' model for cell fate allocation (Figure
889 8C). This model suggests that cell fate allocation is probabilistic and intimately linked to a cells
890 spatiotemporal positioning. In accordance with the binary competence model, cells located
891 within the lateral NPB will give rise to epidermal and placodal fates, whilst those found medially
892 give rise to neural and neural crest fates. However, instead of a binary segregation of the NPB
893 into neural/neural crest and non-neural/placodal domains, we suggest that BLUPs at the NPB

894 are kept in an indeterminate state whilst they continue to co-express factors involved in the
895 specification of alternative lineages. Both our co-expression analysis and previous
896 documentation of heterogeneity at the NPB support this model.

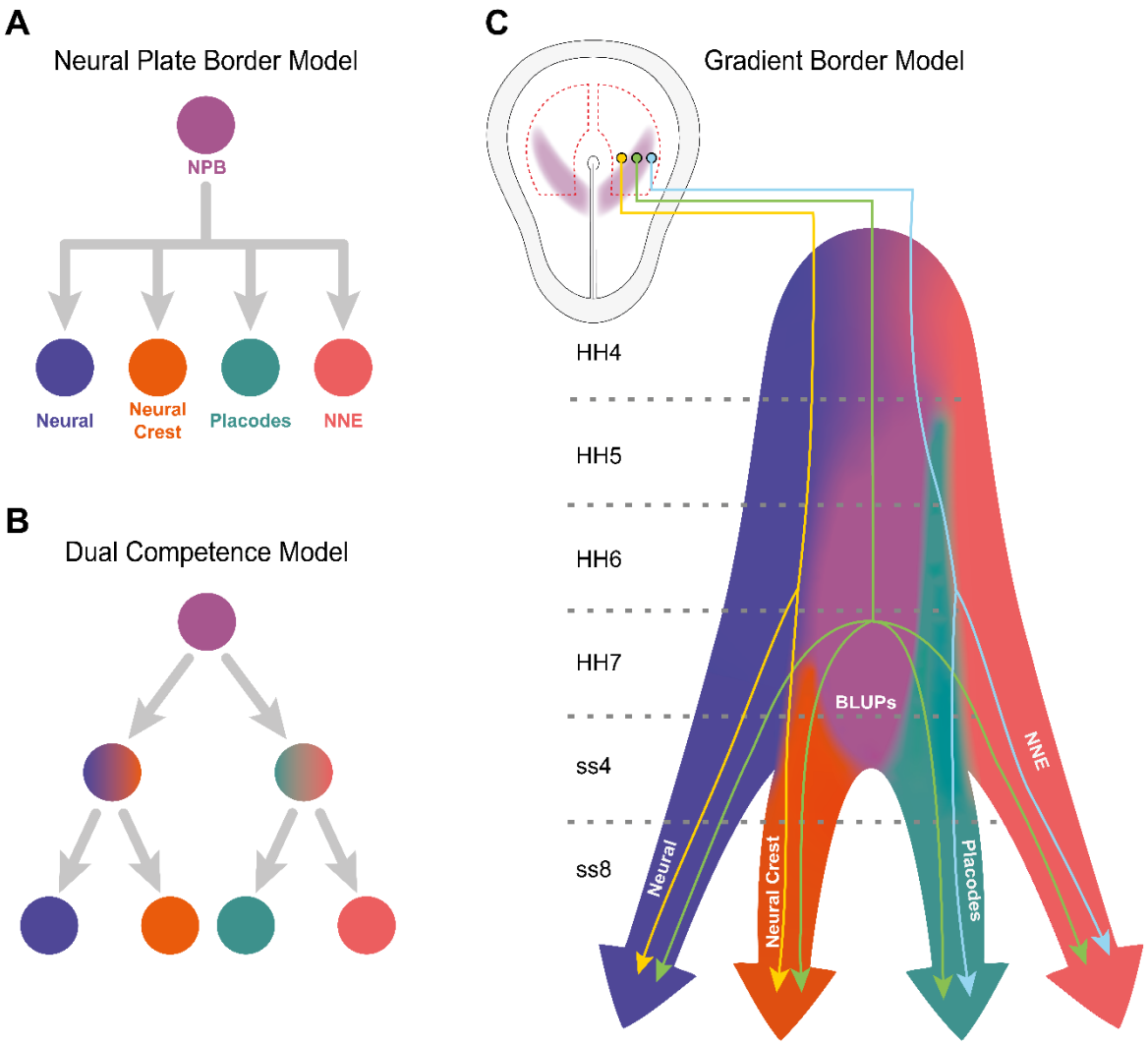

897 **Figure 8. Gradient border model resolves conflicting models of lineage segregation at**
898 **the neural plate border. (A)** Schematic illustrating the neural plate border model. This model
899 illustrates that cells at the neural plate border are multipotent and able to give rise to neural,
900 neural crest, placodal and non-neural ectoderm (NNE) lineages. **(B)** Schematic illustrating the
901 dual competence model. This model suggests that the neural plate border is first defined into
902 non-neural/placodal and neural crest/neural competence domains prior to further subdivision
903 into each of the final four cell lineages. **(C)** Schematic illustrating the gradient border model.
904 This model proposes a probabilistic model of cell fate allocation which is intrinsically linked to
905 the spatiotemporal positioning of a cell. We suggest that cells located within the medial neural
906 plate border (yellow cell lineage) will give rise to neural and neural crest, cells within the lateral
907 neural plate border (blue cell lineage) to non-neural ectoderm and placodes, whilst subsets of
908 cells (including BLUPs) will remain in an indeterminate state and continue to give rise to all
909 four lineages even at late stages of neurulation (green cell lineage). Shaded background
910 colours represent the cell state space.
911

912

913 **Materials and Methods**

914

915 **Data collection and alignment**

916

917 *Single cell dissociation and 10X single-cell mRNA sequencing*

918 Fertilised chicken eggs were incubated at 38°C for 24-32 hours depending upon the
919 developmental stage collected. Embryos were pinned and had the endoderm and mesoderm
920 removed using dispase (10mg/ml) before dissecting the ectodermal region of interest (Figure
921 2A). Multiple embryos from the same stage were pooled prior to dissociation. Samples were
922 then dissociated in 250μl pre-heated FACSmax cell dissociation solution (Amsbio, T200100)
923 with papain (30U/ml; Sigma, P3125) for 20 minutes at 37°C. Samples were gently pipetted
924 every 5 minutes to facilitate dissociation. After dissociation, 250μl resuspension solution was
925 added to prevent any further dissociation (HBSS; non-acetylated BSA (1mg/ml; Invitrogen,
926 10743447); HEPES (0.01M); non-essential amino acids (1x; Thermo Fisher Scientific,
927 11140050); rock inhibitor Y-27632 (10μM; Stemcell Technologies). Cells were passed through
928 a 20μm cell strainer (Miltenyi Biotech, 130-101-812) to remove any debris, before pelleting
929 and resuspending in 500μl resuspension buffer. To remove any dead or dying cells as well as
930 any remaining doublets, 1μl 0.1mg/ml DAPI was added to the cell suspension before FAC
931 sorting. Given the low number of cells obtained from each embryo, samples for each stage
932 were collected over multiple days and stored in 90% MeOH with 10% resuspension solution
933 after FAC sorting. Prior to sequencing, samples from the same stage were pooled and
934 resuspended in DPBS with 0.5% non-acetylated BSA and 0.5U/μl RNAse inhibitor (Roche
935 3335399001).

936

937 Cells underwent single-cell mRNA sequencing at the Francis Crick Institute, London. Library
938 preparation was carried out using the 10x 3' single-cell mRNA v3 kit (10x Genomics), before
939 sequencing on the HiSeq 4000 (Illumina) to a target depth of 50k reads/cell. Samples were
940 sequenced in two batches (batch 1: HH4, HH6, ss4, ss8; batch 2: HH5, HH6, HH7, ss4), with
941 two stages (HH6 and ss4) sequenced in both batches to allow for the correction of any
942 potential batch effects. Data from the first batch has previously been used for the
943 characterisation of neural induction (Trevers et al., 2021) (ArrayExpress accession number:
944 E-MTAB-10408).

945

946 *Read alignment*

947 A custom pipeline was developed in Nextflow (v20.07.1) (Di Tommaso et al., 2017) to handle
948 all GTF processing and read alignment whilst maintaining full reproducibility.

949
950 Prior to scRNAseq alignment, the GalGal6 ensembl 97 GTF file was modified to prefix genes
951 from the Z and W sex chromosomes with their respective chromosome IDs (Z- and W-).
952 Furthermore, we noticed several mitochondrial genes in the GTF were missing their
953 chromosome ID, in turn preventing accurately calculating cell percentage mitochondrial
954 content downstream; mitochondrial genes were therefore also prefixed in the GTF (MT-).
955 Finally, we annotated the key neural crest specifier Snai2 in the GTF
956 (ENSGALG00000030902). Reads were processed and aligned to GalGal6 using CellRanger
957 4.0.0 (10x Genomics).
958
959 The aligned reads from CellRanger (BAM) were re-counted using Velocyto (La Manno et al.,
960 2018) to generate spliced and unspliced counts for each gene, which are used in subsequent
961 RNA velocity analysis.
962
963 **Downstream pre-processing**
964
965 All downstream analysis was wrapped into a custom Nextflow pipeline to simplify re-running
966 the analysis by handling parallel processing of data subsets.
967
968 *Data filtering*
969 Quality control, data filtering, cell clustering, dimensionality reduction and initial data
970 visualisation was carried out using Seurat v4.0.5 (Hao et al., 2021). Data filtering was carried
971 out on each sequencing batch separately before data integration. To ensure the removal of
972 poor-quality cells whilst also minimising over-filtering, we first applied a medium filtering
973 threshold (cells expressing fewer than 1000 genes, more than 6500 genes, or had more than
974 15% mitochondrial content were excluded from subsequent analysis) followed by the removal
975 of remaining poor-quality cell clusters.
976
977 *Dimensionality reduction and clustering*
978 Linear dimensionality reduction was carried out using principal component analysis (PCA).
979 The number of principal components (PCs) used to construct the subsequent shared-nearest-
980 neighbour (SNN) graph was determined unbiasedly, using an approach developed by the
981 Harvard Chan Bioinformatics Core (HBC). First, we calculate the PC at which subsequent PCs
982 contribute less than 5% of standard deviation, and the point where the cumulative variation of
983 PCs exceeds 90%. The larger of these two values is selected. Second, we calculate the PC
984 where the inclusion of consecutive PCs contributes less than 0.1% additional variation. The
985 smaller value from these two steps is selected as a cut-off.

986
987 Louvain clustering was carried out with varying resolutions depending upon the data subset
988 in question. A high clustering resolution (resolution=2) was used to identify poor quality
989 clusters and contaminating cell states. This was to ensure that only poor-quality cells were
990 filtered from the dataset. All other clustering was carried out using a resolution of 0.5.
991
992 *Filtering of poor-quality clusters*
993 Cell quality was measured using unique gene and UMI counts. Clusters in which both metrics
994 fell below the 25th percentile relative to the rest of the dataset were considered poor quality
995 and excluded from further analysis.
996
997 *Data integration*
998 After the removal of poor-quality cells, cells from the two separate batches were integrated
999 into a single full dataset (Figure 2–figure supplement 1H-I). To avoid over-correction and
1000 removal of stage differences, we integrated the data from the two sequencing batches using
1001 STACAS v1.1.0 (Andreatta & Carmona, 2021). This R package allows for alignment of
1002 datasets containing partially overlapping cell states.
1003
1004 *Regressing out confounding variables*
1005 Before downstream analysis, we regressed out percentage mitochondrial content, cell sex,
1006 and cell cycle. After regressing out percentage mitochondrial content, we identified a residual
1007 sex effect whereby cells clustered according to the expression of either W or Z chromosome
1008 genes. This resulted in a duplication of cell clusters, most apparent at HH4 (Figure 2–figure
1009 supplement 1A-D). Cells were k-means clustered according to their expression of W
1010 chromosome genes and classified as either male or female. This classification was used to
1011 regress out cell sex. Cell cycle was observed to have a strong effect on cell clustering and
1012 was therefore also regressed out during data scaling (Figure 2–figure supplement 1E).
1013
1014 *Removal of contaminating clusters*
1015 We found small contaminating clusters of primordial germ cells, blood islands, mesoderm and
1016 endoderm within the dataset (Figure 2–figure supplement 1F, G). To semi-unbiasedly remove
1017 these clusters, we calculated the average expression of candidate markers for each of these
1018 cell states and removed clusters in which the median expression of any of these modules was
1019 greater than the 90th percentile relative to the rest of the dataset (Figure 2–figure supplement
1020 1F'').
1021
1022 **Downstream analysis**

1023

1024 *Unbiased cell classification*

1025 Cell states were classified on each stage independently using a binary knowledge matrix
1026 (Supplementary File 1). First, the full dataset was split by stage and then re-scaled and re-
1027 clustered as described above. Our binary knowledge matrix consists of binarized expression
1028 of 76 genes across 24 cell states. For each gene, published *in situ* hybridisation expression
1029 patterns were used to determine expression within each defined cell state. Given that gene
1030 expression can vary dramatically between stages, and some cell states are known to not be
1031 present at specific timepoints (i.e., delaminating neural crest at HH4), we restricted the
1032 possible cell states at specific stages. At HH4 there were 7 possible cell states, including non-
1033 neural ectoderm (NNE), node, streak, extra-embryonic (EE), early NPB (eNPB), early neural
1034 (eN), early caudal neural (eCN). At HH5 there were 17 potential states, this included all cell
1035 states in the binary knowledge matrix, except for the later counterparts to the earlier cell states
1036 which are ventral forebrain (vFB), forebrain (FB), midbrain (MB), hindbrain (HB), neural crest
1037 (NC), delaminating neural crest (dNC) and presumptive epidermis (pEpi). At HH6 we included
1038 the same cell states as HH5 except for EE and eNPB given that no cell clusters were classified
1039 as such at HH5. For stages HH7, ss4 and ss8 we included 17 cell states, excluding the
1040 following states which are only found at earlier stages (NNE, node, streak, eN, eCN, eNPB,
1041 EE).

1042

1043 For each cell, we calculated the average scaled expression of the genes expressed in each
1044 cell state according to our binary knowledge matrix. Cell clusters were then assigned a cell
1045 state, depending on which cell state exhibited the highest median expression in that given cell
1046 cluster. Assigned cell states at each of the 6 sampled developmental stages were then
1047 transferred to the full dataset.

1048

1049 *Gene module identification and filtering*

1050 To calculate groups of highly correlated genes, we first filtered genes which do not correlate
1051 (Spearman correlation < 0.3) with at least 3 other genes. Then we calculated gene modules
1052 using the Antler R package (Delile et al., 2019), which iteratively clusters genes hierarchically
1053 based on their gene-gene Spearman correlation. After each iteration, gene modules were
1054 filtered to remove gene modules which are not highly expressed (expressed in fewer than 10
1055 cells) or which do not show consistent high expression across genes (fewer than 40% of genes
1056 in the module are expressed after binarization). Gene modules were calculated on different
1057 subsets of cells: the full dataset (Figure 4E and Figure 4–figure supplement 1A), ss8 (Figure
1058 5A and Figure 5–figure supplement 1A), and the NPB subset (Figure 7E). Calculating gene

1059 modules on different subsets allowed us to zoom in on specific aspects of ectodermal lineage
1060 segregation.
1061
1062 Many genes correlate across the dataset, but do not show differential expression between cell
1063 states and therefore do not provide useful information regarding lineage segregation.
1064 Therefore, to identify which gene modules correlate with lineage segregation, modules were
1065 filtered to only include those in which more than 50% of their genes were differentially
1066 expressed (logFC > 0.5, adjusted p-value < 0.001) in at least one cell state relative to the rest
1067 of the dataset. For the NPB subset, this filtering of differential expression was just between
1068 the neural crest (NC, dNC) and placodal (aPPR, pPPR, PPR) states rather than between all
1069 cell states (logFC > 0.25, adjusted p-value < 0.001).
1070
1071 To remove gene modules which correlate with technical variation, we filtered those in which
1072 more than 50% their genes showed differential expression between sequencing batches
1073 (logFC > 0.25, adjusted p-value <0.001).
1074
1075 For the gene modules calculated on the full dataset, we were particularly interested in gene
1076 modules that segregated into one of the three lineages (neural, neural crest or placodal) at
1077 later stages. To focus our analysis on these gene modules, we applied an additional filtering
1078 step to only keep gene modules in which more than 50% of genes were differentially
1079 expressed between one of the three lineages at ss8 (logFC > 0.25, adjusted p-value <0.001).
1080 After filtering 9 gene modules remained (Figure 4–figure supplement 1A, Figure 4–Source
1081 Data 1). Modules were further manually filtered for visualisation (Figure 4E).
1082
1083 For the gene modules calculated on the NPB subset we wanted to focus on the co-expression
1084 and sequential activation of gene modules that contain well-characterised neural crest and
1085 PPR markers. We therefore further filtered NPB gene modules to include only those that had
1086 genes that were defined within neural crest, delaminating neural crest or PPR cell states in
1087 the binary knowledge matrix. After this final filtering step, 7 gene modules remained (Figure
1088 7E, Figure 7–Source Data 1).
1089
1090 *Identification of undetermined cells at the NPB*
1091 To identify which cells expressed competing pan-placodal and pan-neural crest modules at
1092 similar levels, we calculated the average expression (normalised counts) of these two gene
1093 modules in each cell and then ordered cells by their ratio of pan-placodal to pan-neural crest
1094 module expression. Cells were then grouped into 10 evenly sized bins and visualised on
1095 UMAPs.

1096

1097 *Co-expression distribution plots*

1098 To investigate the distribution of co-expression between cells, co-expression histograms were
1099 plotted (Figure 5I). Co-expression values were calculated by multiplying the average
1100 normalised expression of the pan-placodal and pan-neural crest gene modules.

1101

1102 *Co-expression visualisation*

1103 The average normalised expression of each gene module was scaled between 0 and 1. A
1104 100x100 two-colour matrix was created using Seurat's BlendMatrix function. Each cell was
1105 assigned a colour from this matrix based on their scaled average expression of the gene
1106 modules (Figure 5H). Only cells which express both modules above a threshold of 0.3 after
1107 scaling were visualised.

1108

1109 *RNA velocity*

1110 Spliced and unspliced matrices obtained from Velocyto (La Manno et al., 2018) (see *Read*
1111 *Alignment*) were analysed using scVelo (Bergen et al., 2020) to generate cell velocity vectors.
1112 Velocyto matrices were intersected with each of the data subsets generated in Seurat. First
1113 and second order moments were then calculated for each cell across its 20 nearest
1114 neighbours using the top 20 PCs. RNA velocity was ran using the dynamical model whilst
1115 accounting for differential kinetics; this allows for differential splicing rates between genes as
1116 well as differential splicing kinetics between cell states.

1117

1118 Latent time was calculated and used downstream as a measure of a cell's internal clock. When
1119 calculating latent time, cells were rooted to the earliest timepoint present in the data subset;
1120 in cases where only one stage was present, the cell root was calculated automatically. For all
1121 latent time estimates, we used a diffusion weighting of 0.2.

1122

1123 *Modelling gene expression dynamics*

1124 Lineage inference was calculated using CellRank, which uses a probabilistic approach to
1125 assign cell lineage (Lange et al., 2022). Cell transition matrices were calculated using RNA
1126 velocity (0.8 weighting) and nearest neighbour graph (0.2 weighting) kernels. A softmax scale
1127 of 4 was set to prevent transitions tending towards orthogonality. When predicting cell
1128 transitions, terminal states were specified according to the lineages which we were wanting to
1129 model gene dynamics across. For the full dataset, we predicted cell transitions towards either
1130 neural, placodal or neural crest lineages. Terminal states were specified as: delaminating
1131 neural crest and neural crest cell states at ss4 and ss8 for the neural crest lineage; hindbrain,
1132 midbrain, and forebrain cell states at ss4 and ss8 for the neural lineage; anterior PPR,

1133 posterior PPR and PPR cell states at ss4 and ss8 for the placodal lineage (Figure 4–figure
1134 supplement 1C). For our NPB subset we predicted cell transitions towards either placodal or
1135 neural crest lineages, with terminal states specified as: delaminating neural crest and neural
1136 crest cell states at ss8 for the neural crest lineage; aPPR and PPR cell states at ss8 for the
1137 placodal lineage.
1138
1139 Gene expression dynamics were calculated by fitting general additive models (GAM), which
1140 modelled scaled gene expression as a function of latent time using the mgcv package in R.
1141 Lineage absorption probability obtained from CellRank were used to weight a GAM for each
1142 of the predicted lineages. To generate a smoothed prediction of gene expression change, a
1143 cubic spline was fitted with knots=4. When modelling the dynamics of entire gene modules,
1144 all genes within a given module were included in the GAM.
1145
1146 *Modelling mediolateral gene expression patterns from scRNAseq data*
1147 Following principal component analysis of cells at HH7, the order of cell states across the
1148 inverse of PC 1 were found to reflect the M-L positioning of cells *in vivo*. Genes which were.
1149 To model the expression of placodal and neural crest markers across the M-L axis, GAMs
1150 were fitted for the scaled expression of each gene across PC 1 using ggplot2::geom_smooth.
1151
1152 **Fluorescent *in situ* hybridisation chain reaction**
1153
1154 Hybridisation chain reaction v3 (HCR) was carried out as previously described (Buzzi et al.,
1155 2022; Choi et al., 2018). Embryos were fixed in 4% PFA for 1h at room temperature,
1156 dehydrated in a series of methanol in PBT, and stored overnight at -20°C. Samples were
1157 rehydrated and treated with proteinase-K for 3 min (20 mg/mL). Next samples were post-fixed
1158 in 4% PFA for 20 min and sequentially washed on ice for 5 min in PBS, 1:1 PBT/5×SSC
1159 (5×sodium chloride sodium citrate, 0.1% Tween-20), and 5×SSC. Samples were then pre-
1160 hybridised in hybridisation buffer for 5 min on ice, followed by 30 min at 37°C. Next, samples
1161 were hybridised overnight at 37°C with HCR probes in hybridisation buffer (4 pmol/mL).
1162 Excess probe was washed off with 15 min washes in probe wash buffer at 37°C, before
1163 preamplification in amplification buffer at room temperature for 5 min. Hairpins (30 pmol) were
1164 incubated at 95°C for 90 s and left to cool to room temperature for 30 min before being added
1165 to the amplification buffer. Samples were then incubated with the hairpin/amplification buffer
1166 solution overnight at room temperature. Excess hairpins were washed off with two 5 min and
1167 two 30 min washes in 5×SSC. After a 5 min incubation in DAPI (10 mg/mL), samples were
1168 washed 3 times for 10 min in 5×SSC before being imaged using a Leica SP5 laser scanning
1169 confocal inverted microscope using the LAS AF software.

1170

1171 Intensity measurements were calculated by taking the sum of slices from the image Z-stacks
1172 taken at three anteroposterior levels in ImageJ. The three intensity measurements were then
1173 independently scaled (Z-score) for each gene to allow relative measurements of gene
1174 expression across the anteroposterior axis. Transverse virtual sections across the
1175 anteroposterior axis were obtained using the Imaris 9.3.1 software. 10 µm sections were
1176 generated with the orthogonal slice tool.

1177

1178

1179 **Data availability and reproducibility**

1180

1181 10x single cell RNAseq was carried out in two batches and is available under two separate
1182 accession numbers (ArrayExpress: E-MTAB-10408 and E-MTAB-1144). Our NGS alignments
1183 and downstream analysis have been wrapped into custom Nextflow pipelines allowing for full
1184 reproducibility. For the code used in this analysis, including links to our Docker containers, see
1185 our GitHub repository at https://github.com/alexthiery/10x_neural_plate_border.

1186

1187 **Acknowledgements**

1188

1189 We thank Teresa Rayon for assistance with establishing the single cell dissociation protocol
1190 and the Advanced Sequencing Facility at the Francis Crick Institute for the single cell RNA
1191 sequencing. We would also like to thank Igor Adameyko and Artem Artemov for guidance on
1192 co-expression analysis, Chantal Hubens for technical support, Alessandra Vigilante and Sami
1193 Leino for comments on the manuscript, and Streit and Luscombe lab groups for helpful
1194 discussions. This work was supported by the Wellcome Trust (108874/B/15/Z), the BBSRC
1195 (BB/S005536/1; BB/R006342/1) and in part by the Francis Crick Institute which receives its
1196 core funding from Cancer Research UK (FC001051), the UK Medical Research Council
1197 (FC001051), and the Wellcome Trust (FC001051). For the purpose of Open Access, the
1198 author has applied a CC BY public copyright license to any Author Accepted Manuscript
1199 version arising from this submission.

1200

1201 **Author contributions**

1202

1203 A.S., J.B., A.T. and A.L.B. designed study. A.T., A.L.B., E.H. and A.S. collected samples and
1204 processed for scRNAseq. A.T., C.C. developed analysis pipeline and carried out data
1205 alignment. A.T. and E.H. carried out the downstream computational analysis of scRNAseq
1206 data, while A.L.B. and A.T. performed HCR analysis. A.T., A.L.B., E.H., N.L., J.B. and A.S.

interpreted the results. A.T., A.L.B., E.H. and A.S. made figures and wrote the manuscript. All authors provided feedback on the manuscript.

1210 **References**

1211 Adams, M. S., Gammill, L. S., & Bronner-Fraser, M. (2008). Discovery of transcription factors
1212 and other candidate regulators of neural crest development. *Dev Dyn, 237*(4), 1021-
1213 1033. doi:10.1002/dvdy.21513

1214 Ahrens, K., & Schlosser, G. (2005). Tissues and signals involved in the induction of placodal
1215 Six1 expression in Xenopus laevis. *Dev Biol, 288*(1), 40-59.

1216 Andreatta, M., & Carmona, S. J. (2021). STACAS: Sub-Type Anchor Correction for Alignment
1217 in Seurat to integrate single-cell RNA-seq data. *Bioinformatics, 37*(6), 882-884.
1218 doi:10.1093/bioinformatics/btaa755

1219 Baker, C. V., & Bronner-Fraser, M. (1997a). The origins of the neural crest. Part I: embryonic
1220 induction. *Mech Dev, 69*(1-2), 3-11. doi:10.1016/s0925-4773(97)00132-9

1221 Baker, C. V., & Bronner-Fraser, M. (1997b). The origins of the neural crest. Part II: an
1222 evolutionary perspective. *Mech Dev, 69*(1-2), 13-29. doi:10.1016/s0925-
1223 4773(97)00129-9

1224 Baker, C. V., & Bronner-Fraser, M. (2001). Vertebrate cranial placodes I. Embryonic induction.
1225 *Dev Biol, 232*(1), 1-61. doi:10.1006/dbio.2001.0156

1226 Barembaum, M., & Bronner-Fraser, M. (2007). Spalt4 mediates invagination and otic placode
1227 gene expression in cranial ectoderm. *Development, 134*(21), 3805-3814.
1228 doi:10.1242/dev.02885

1229 Barth, K. A., Kishimoto, Y., Rohr, K. B., Seydler, C., Schulte-Merker, S., & Wilson, S. W.
1230 (1999). Bmp activity establishes a gradient of positional information throughout the
1231 entire neural plate. *Development, 126*(22), 4977-4987.

1232 Basch, M. L., Bronner-Fraser, M., & Garcia-Castro, M. I. (2006). Specification of the neural
1233 crest occurs during gastrulation and requires Pax7. *Nature, 441*(7090), 218-222.

1234 Bell, G. W., Yatskievych, T. A., & Antin, P. B. (2004). GEISHA, a whole-mount in situ
1235 hybridization gene expression screen in chicken embryos. *Dev Dyn, 229*(3), 677-687.
1236 doi:10.1002/dvdy.10503

1237 Bergen, V., Lange, M., Peidli, S., Wolf, F. A., & Theis, F. J. (2020). Generalizing RNA velocity
1238 to transient cell states through dynamical modeling. *Nat Biotechnol, 38*(12), 1408-
1239 1414. doi:10.1038/s41587-020-0591-3

1240 Betancur, P., Bronner-Fraser, M., & Sauka-Spengler, T. (2010). Assembling neural crest
1241 regulatory circuits into a gene regulatory network. *Annu Rev Cell Dev Biol, 26*, 581-
1242 603. doi:10.1146/annurev.cellbio.042308.113245

1243 Bhat, N., Kwon, H. J., & Riley, B. B. (2013). A gene network that coordinates preplacodal
1244 competence and neural crest specification in zebrafish. *Dev Biol, 373*(1), 107-117.
1245 doi:10.1016/j.ydbio.2012.10.012

1246 Bhattacharyya, S., Bailey, A. P., Bronner-Fraser, M., & Streit, A. (2004). Segregation of lens
1247 and olfactory precursors from a common territory: cell sorting and reciprocity of Dlx5
1248 and Pax6 expression. *Dev Biol, 271*(2), 403-414. doi:10.1016/j.ydbio.2004.04.010

1249 Brugmann, S. A., Pandur, P. D., Kenyon, K. L., Pignoni, F., & Moody, S. A. (2004). Six1
1250 promotes a placodal fate within the lateral neurogenic ectoderm by functioning as both
1251 a transcriptional activator and repressor. *Development, 131*(23), 5871-5881.

1252 Buitrago-Delgado, E., Nordin, K., Rao, A., Geary, L., & LaBonne, C. (2015). Shared regulatory
1253 programs suggest retention of blastula-stage potential in neural crest cells. *Science,*
1254 *348*(6241), 1332-1335. doi:10.1126/science.aaa3655

1255 Buzzi, A. L., Chen, J., Thiery, A., Delile, J., & Streit, A. (2022). Sox8 remodels the cranial
1256 ectoderm to generate the ear. *Proceedings of the National Academy of Sciences,*
1257 *119*(28), e2118938119. doi:doi:10.1073/pnas.2118938119

1258 Chapman, S. C., Schubert, F. R., Schoenwolf, G. C., & Lumsden, A. (2002). Analysis of spatial
1259 and temporal gene expression patterns in blastula and gastrula stage chick embryos.
1260 *Dev Biol, 245*(1), 187-199. doi:10.1006/dbio.2002.0641

1261 Chen, B., Kim, E.-H., & Xu, P.-X. (2009). Initiation of olfactory placode development and
1262 neurogenesis is blocked in mice lacking both Six1 and Six4. *Developmental Biology,*
1263 *326*(1), 75-85.

1264 Choi, H. M. T., Schwarzkopf, M., Fornace, M. E., Acharya, A., Artavanis, G., Stegmaier, J.,
1265 Cunha, A., & Pierce, N. A. (2018). Third-generation in situ hybridization chain reaction:
1266 multiplexed, quantitative, sensitive, versatile, robust. *Development, 145*(12).
1267 doi:10.1242/dev.165753

1268 Christophorou, N. A., Bailey, A. P., Hanson, S., & Streit, A. (2009). Activation of Six1 target
1269 genes is required for sensory placode formation. *Dev Biol, 336*(2), 327-336.

1270 Delile, J., Rayon, T., Melchionda, M., Edwards, A., Briscoe, J., & Sagner, A. (2019). Single
1271 cell transcriptomics reveals spatial and temporal dynamics of gene expression in the
1272 developing mouse spinal cord. *Development, 146*(12). doi:10.1242/dev.173807

1273 Di Tommaso, P., Chatzou, M., Floden, E. W., Barja, P. P., Palumbo, E., & Notredame, C.
1274 (2017). Nextflow enables reproducible computational workflows. *Nat Biotechnol, 35*(4),
1275 316-319. doi:10.1038/nbt.3820

1276 Ezin, A. M., Fraser, S. E., & Bronner-Fraser, M. (2009). Fate map and morphogenesis of
1277 presumptive neural crest and dorsal neural tube. *Dev Biol, 330*(2), 221-236.
1278 doi:10.1016/j.ydbio.2009.03.018

1279 Garcia-Castro, M. I., Marcelle, C., & Bronner-Fraser, M. (2002). Ectodermal Wnt function as
1280 a neural crest inducer. *Science, 297*(5582), 848-851.

1281 Grocott, T., Tambalo, M., & Streit, A. (2012). The peripheral sensory nervous system in the
1282 vertebrate head: a gene regulatory perspective. *Dev Biol, 370*(1), 3-23.
1283 doi:10.1016/j.ydbio.2012.06.028

1284 Hao, Y., Hao, S., Andersen-Nissen, E., Mauck, W. M., III., Zheng, S., Butler, A., Lee, M. J.,
1285 Wilk, A. J., Darby, C., Zager, M., Hoffman, P., Stoeckius, M., Papalexi, E., Mimitou, E.
1286 P., Jain, J., Srivastava, A., Stuart, T., Fleming, L. M., Yeung, B., Rogers, A. J.,
1287 McElrath, J. M., Blish, C. A., Gottardo, R., Smibert, P., & Satija, R. (2021). Integrated
1288 analysis of multimodal single-cell data. *Cell, 184*(13), 3573-3587 e3529.
1289 doi:10.1016/j.cell.2021.04.048

1290 Heeg-Truesdell, E., & LaBonne, C. (2006). Neural induction in Xenopus requires inhibition of
1291 Wnt-beta-catenin signaling. *Developmental Biology, 298*(1), 71-86.

1292 Hemmati-Brivanlou, A., Kelly, O. G., & Melton, D. A. (1994). Follistatin, an antagonist of activin,
1293 is expressed in the Spemann organizer and displays direct neuralizing activity. *Cell,*
1294 *77*(2), 283-295.

1295 Hidalgo-Sanchez, M., Millet, S., Bloch-Gallego, E., & Alvarado-Mallart, R. M. (2005).
1296 Specification of the meso-isthmo-cerebellar region: the Otx2/Gbx2 boundary. *Brain*
1297 *Res Brain Res Rev, 49*(2), 134-149. doi:10.1016/j.brainresrev.2005.01.010

1298 Hidalgo-Sanchez, M., Millet, S., Simeone, A., & Alvarado-Mallart, R. M. (1999). Comparative
1299 analysis of Otx2, Gbx2, Pax2, Fgf8 and Wnt1 gene expressions during the formation
1300 of the chick midbrain/hindbrain domain. *Mech Dev, 81*(1-2), 175-178.
1301 doi:10.1016/s0925-4773(98)00224-x

Hintze, M., Prajapati, R. S., Tambalo, M., Christophorou, N. A. D., Anwar, M., Grocott, T., & Streit, A. (2017). Cell interactions, signals and transcriptional hierarchy governing placode progenitor induction. *Development, 144*(15), 2810-2823. doi:10.1242/dev.147942

Hollyday, M., McMahon, J. A., & McMahon, A. P. (1995). Wnt expression patterns in chick embryo nervous system. *Mech Dev, 52*(1), 9-25. doi:10.1016/0925-4773(95)00385-e

Hong, C. S., & Saint-Jeannet, J. P. (2007). The activity of Pax3 and Zic1 regulates three distinct cell fates at the neural plate border. *Mol Biol Cell, 18*(6), 2192-2202. doi:10.1091/mbc.e06-11-1047

Kwon, H. J., Bhat, N., Sweet, E. M., Cornell, R. A., & Riley, B. B. (2010). Identification of early requirements for preplacodal ectoderm and sensory organ development. *PLoS Genet, 6*(9). doi:10.1371/journal.pgen.1001133

La Manno, G., Soldatov, R., Zeisel, A., Braun, E., Hochgerner, H., Petukhov, V., Lidschreiber, K., Kastriti, M. E., Lonnerberg, P., Furlan, A., Fan, J., Borm, L. E., Liu, Z., van Bruggen, D., Guo, J., He, X., Barker, R., Sundstrom, E., Castelo-Branco, G., Cramer, P., Adameyko, I., Linnarsson, S., & Kharchenko, P. V. (2018). RNA velocity of single cells. *Nature, 560*(7719), 494-498. doi:10.1038/s41586-018-0414-6

Lange, M., Bergen, V., Klein, M., Setty, M., Reuter, B., Bakhti, M., Lickert, H., Ansari, M., Schniering, J., Schiller, H. B., Pe'er, D., & Theis, F. J. (2022). CellRank for directed single-cell fate mapping. *Nat Methods*. doi:10.1038/s41592-021-01346-6

Liberatore, C. M., Searcy-Schrick, R. D., & Yutzey, K. E. (2000). Ventricular expression of tbx5 inhibits normal heart chamber development. *Dev Biol, 223*(1), 169-180. doi:10.1006/dbio.2000.9748

Liem, K. F., Jr., Tremml, G., Roelink, H., & Jessell, T. M. (1995). Dorsal differentiation of neural plate cells induced by BMP-mediated signals from epidermal ectoderm. *Cell, 82*(6), 969-979.

Linker, C., & Stern, C. D. (2004). Neural induction requires BMP inhibition only as a late step, and involves signals other than FGF and Wnt antagonists. *Development, 131*(22), 5671-5681.

Litsiou, A., Hanson, S., & Streit, A. (2005). A balance of FGF, Wnt and BMP signalling positions the future placode territory in the head. *Development, 132*, 4051-4062.

Londin, E. R., Niemiec, J., & Sirotkin, H. I. (2005). Chordin, FGF signalling, and mesodermal factors cooperate in zebrafish neural induction. *Dev Biol, 279*(1), 1-19.

Marchant, L., Linker, C., Ruiz, P., Guerrero, N., & Mayor, R. (1998). The inductive properties of mesoderm suggest that the neural crest cells are specified by a BMP gradient. *Dev Biol, 198*(2), 319-329.

McLarren, K. W., Litsiou, A., & Streit, A. (2003). DLX5 positions the neural crest and preplacode region at the border of the neural plate. *Dev Biol, 259*(1), 34-47. doi:10.1016/s0012-1606(03)00177-5

Mehdizadeh, T., Majumdar, H. D., Ahsan, S., Tavares, A. L. P., & Moody, S. A. (2021). Mutations in SIX1 Associated with Branchio-oto-Renal Syndrome (BOR) Differentially Affect Otic Expression of Putative Target Genes. *J Dev Biol, 9*(3). doi:10.3390/jdb9030025

Milet, C., Maczkowiak, F., Roche, D. D., & Monsoro-Burq, A. H. (2013). Pax3 and Zic1 drive induction and differentiation of multipotent, migratory, and functional neural crest in Xenopus embryos. *Proc Natl Acad Sci U S A, 110*(14), 5528-5533. doi:10.1073/pnas.1219124110

1349 Monsoro-Burq, A. H. (2015). PAX transcription factors in neural crest development. *Semin*
1350 *Cell Dev Biol, 44*, 87-96. doi:10.1016/j.semcdb.2015.09.015

1351 Monsoro-Burq, A. H., Fletcher, R. B., & Harland, R. M. (2003). Neural crest induction by
1352 paraxial mesoderm in Xenopus embryos requires FGF signals. *Development, 130*(14),
1353 3111-3124.

1354 Monsoro-Burq, A. H., Wang, E., & Harland, R. (2005). Msx1 and Pax3 cooperate to mediate
1355 FGF8 and WNT signals during Xenopus neural crest induction. *Dev Cell, 8*(2), 167-
1356 178. doi:10.1016/j.devcel.2004.12.017

1357 Ohuchi, H., Tomonari, S., Itoh, H., Mikawa, T., & Noji, S. (1999). Identification of chick rax/rx
1358 genes with overlapping patterns of expression during early eye and brain development.
1359 *Mech Dev, 85*(1-2), 193-195. doi:10.1016/s0925-4773(99)00094-5

1360 Ota, K., Nagai, H., & Sheng, G. (2007). Expression and hypoxic regulation of hif1alpha and
1361 hif2alpha during early blood and endothelial cell differentiation in chick. *Gene Expr*
1362 *Patterns, 7*(7), 761-766. doi:10.1016/j.modgep.2007.05.007

1363 Ozaki, H., Nakamura, K., Funahashi, J., Ikeda, K., Yamada, G., Tokano, H., Okamura, H. O.,
1364 Kitamura, K., Muto, S., Kotaki, H., Sudo, K., Horai, R., Iwakura, Y., & Kawakami, K.
1365 (2004). Six1 controls patterning of the mouse otic vesicle. *Development, 131*(3), 551-
1366 562.

1367 Patthey, C., Gunhaga, L., & Edlund, T. (2008). Early development of the central and peripheral
1368 nervous systems is coordinated by Wnt and BMP signals. *PLoS ONE, 3*(2), e1625.
1369 doi:10.1371/journal.pone.0001625

1370 Patthey, C., Schlosser, G., & Shimeld, S. M. (2014). The evolutionary history of vertebrate
1371 cranial placodes--I: cell type evolution. *Dev Biol, 389*(1), 82-97.
1372 doi:10.1016/j.ydbio.2014.01.017

1373 Paxton, C. N., Bleyl, S. B., Chapman, S. C., & Schoenwolf, G. C. (2010). Identification of
1374 differentially expressed genes in early inner ear development. *Gene Expr Patterns,*
1375 *10*(1), 31-43. doi:10.1016/j.gep.2009.11.002

1376 Pera, E., Stein, S., & Kessel, M. (1999). Ectodermal patterning in the avian embryo: epidermis
1377 versus neural plate. *Development, 126*(1), 63-73.

1378 Pieper, M., Ahrens, K., Rink, E., Peter, A., & Schlosser, G. (2012). Differential distribution of
1379 competence for panplacodal and neural crest induction to non-neural and neural
1380 ectoderm. *Development, 139*(6), 1175-1187. doi:10.1242/dev.074468

1381 Pla, P., & Monsoro-Burq, A. H. (2018). The neural border: Induction, specification and
1382 maturation of the territory that generates neural crest cells. *Dev Biol, 444 Suppl 1*, S36-
1383 S46. doi:10.1016/j.ydbio.2018.05.018

1384 Plouhinec, J. L., Roche, D. D., Pegoraro, C., Figueiredo, A. L., Maczkowiak, F., Brunet, L. J.,
1385 Milet, C., Vert, J. P., Pollet, N., Harland, R. M., & Monsoro-Burq, A. H. (2014). Pax3
1386 and Zic1 trigger the early neural crest gene regulatory network by the direct activation
1387 of multiple key neural crest specifiers. *Dev Biol, 386*(2), 461-472.
1388 doi:10.1016/j.ydbio.2013.12.010

1389 Prasad, M. S., Charney, R. M., & Garcia-Castro, M. I. (2019). Specification and formation of
1390 the neural crest: Perspectives on lineage segregation. *Genesis, 57*(1), e23276.
1391 doi:10.1002/dvg.23276

1392 Prasad, M. S., Sauka-Spengler, T., & LaBonne, C. (2012). Induction of the neural crest state:
1393 control of stem cell attributes by gene regulatory, post-transcriptional and epigenetic
1394 interactions. *Dev Biol, 366*(1), 10-21. doi:10.1016/j.ydbio.2012.03.014

Reichert, S., Randall, R. A., & Hill, C. S. (2013). A BMP regulatory network controls ectodermal cell fate decisions at the neural plate border. *Development, 140*(21), 4435-4444. doi:10.1242/dev.098707

Rex, M., Orme, A., Uwanogho, D., Tointon, K., Wigmore, P. M., Sharpe, P. T., & Scotting, P. J. (1997). Dynamic expression of chicken Sox2 and Sox3 genes in ectoderm induced to form neural tissue. *Dev Dyn, 209*(3), 323-332. doi:10.1002/(SICI)1097-0177(199707)209:3<323::AID-AJA7>3.0.CO;2-K

Roellig, D., Tan-Cabugao, J., Esaian, S., & Bronner, M. E. (2017). Dynamic transcriptional signature and cell fate analysis reveals plasticity of individual neural plate border cells. *Elife, 6*. doi:10.7554/eLife.21620

Rothstein, M., & Simoes-Costa, M. (2020). Heterodimerization of TFAP2 pioneer factors drives epigenomic remodeling during neural crest specification. *Genome Res, 30*(1), 35-48. doi:10.1101/gr.249680.119

Sasai, Y., Lu, B., Steinbeisser, H., & De Robertis, E. M. (1995). Regulation of neural induction by the Chd and Bmp-4 antagonistic patterning signals in Xenopus. *Nature, 376*(6538), 333-336.

Schlosser, G. (2006). Induction and specification of cranial placodes. *Dev Biol, 294*(2), 303-351. doi:10.1016/j.ydbio.2006.03.009

Schlosser, G. (2014). Early embryonic specification of vertebrate cranial placodes. *Wiley Interdiscip Rev Dev Biol, 3*(5), 349-363. doi:10.1002/wdev.142

Schlosser, G., Awtry, T., Brugmann, S. A., Jensen, E. D., Neilson, K., Ruan, G., Stammler, A., Voelker, D., Yan, B., Zhang, C., Klymkowsky, M. W., & Moody, S. A. (2008). Eya1 and Six1 promote neurogenesis in the cranial placodes in a SoxB1-dependent fashion. *Dev Biol, 320*(1), 199-214. doi:10.1016/j.ydbio.2008.05.523

Sheng, G., & Stern, C. D. (1999). Gata2 and Gata3: novel markers for early embryonic polarity and for non-neural ectoderm in the chick embryo. *Mech Dev, 87*(1-2), 213-216. doi:10.1016/s0925-4773(99)00150-1

Simoes-Costa, M., & Bronner, M. E. (2015). Establishing neural crest identity: a gene regulatory recipe. *Development, 142*(2), 242-257. doi:10.1242/dev.105445

Soldatov, R., Kaucka, M., Kastriti, M. E., Petersen, J., Chontorotzea, T., Englmaier, L., Akkuratova, N., Yang, Y., Haring, M., Dyachuk, V., Bock, C., Farlik, M., Piacentino, M. L., Boismoreau, F., Hilscher, M. M., Yokota, C., Qian, X., Nilsson, M., Bronner, M. E., Croci, L., Hsiao, W. Y., Guertin, D. A., Brunet, J. F., Consalez, G. G., Ernfors, P., Fried, K., Kharchenko, P. V., & Adameyko, I. (2019). Spatiotemporal structure of cell fate decisions in murine neural crest. *Science, 364*(6444). doi:10.1126/science.aas9536

Steventon, B., Araya, C., Linker, C., Kuriyama, S., & Mayor, R. (2009). Differential requirements of BMP and Wnt signalling during gastrulation and neurulation define two steps in neural crest induction. *Development, 136*(5), 771-779. doi:10.1242/dev.029017

Steventon, B., Mayor, R., & Streit, A. (2012). Mutual repression between Gbx2 and Otx2 in sensory placodes reveals a general mechanism for ectodermal patterning. *Dev Biol, 367*(1), 55-65. doi:10.1016/j.ydbio.2012.04.025

Streit, A. (2002). Extensive cell movements accompany formation of the otic placode. *Dev Biol, 249*(2), 237-254. doi:10.1006/dbio.2002.0739

Streit, A., Berliner, A. J., Papanayotou, C., Sirulnik, A., & Stern, C. D. (2000). Initiation of neural induction by FGF signalling before gastrulation. *Nature, 406*(6791), 74-78.

Streit, A., Lee, K. J., Woo, I., Roberts, C., Jessell, T. M., & Stern, C. D. (1998). Chordin regulates primitive streak development and the stability of induced neural cells, but is not sufficient for neural induction in the chick embryo. *Development, 125*(3), 507-519.

Streit, A., & Stern, C. D. (1999). Establishment and maintenance of the border of the neural plate in the chick: involvement of FGF and BMP activity. *Mech Dev, 82*(1-2), 51-66.

Stuhlmiller, T. J., & García-Castro, M. I. (2012). FGF/MAPK signaling is required in the gastrula epiblast for avian neural crest induction. *Development, 139*(2), 289-300. doi:10.1242/dev.070276

Stundl, J., Bertucci, P. Y., Lauri, A., Arendt, D., & Bronner, M. E. (2021). Evolution of new cell types at the lateral neural border. *Curr Top Dev Biol, 141*, 173-205. doi:10.1016/bs.ctdb.2020.11.005

Thiery, A., Buzzi, A. L., & Streit, A. (2020). Cell fate decisions during the development of the peripheral nervous system in the vertebrate head. *Curr Top Dev Biol, 139*, 127-167. doi:10.1016/bs.ctdb.2020.04.002

Trevers, K. E., Lu, H. C., Yang, Y., Thiery, A., Strobl, A. C., Pálinkášová, B., de Oliveira, N. M. M., de Almeida, I. M., Khan, M. A. F., Moncaut, N., Luscombe, N. M., Dale, L., Streit, A., & Stern, C. D. (2021). A gene regulatory network for neural induction. *bioRxiv*, 2021.2004.2016.440164. doi:10.1101/2021.04.16.440164

Trevers, K. E., Prajapati, R. S., Hintze, M., Stower, M. J., Strobl, A. C., Tambalo, M., Ranganathan, R., Moncaut, N., Khan, M. A. F., Stern, C. D., & Streit, A. (2018). Neural induction by the node and placode induction by head mesoderm share an initial state resembling neural plate border and ES cells. *Proc Natl Acad Sci U S A, 115*(2), 355-360. doi:10.1073/pnas.1719674115

Wakamatsu, Y., Endo, Y., Osumi, N., & Weston, J. A. (2004). Multiple roles of Sox2, an HMG-box transcription factor in avian neural crest development. *Dev Dyn, 229*(1), 74-86. doi:10.1002/dvdy.10498

Williams, R. M., Lukoseviciute, M., Sauka-Spengler, T., & Bronner, M. E. (2022). Single-cell atlas of early chick development reveals gradual segregation of neural crest lineage from the neural plate border during neurulation. *Elife, 11*. doi:10.7554/eLife.74464

Wilson, S. I., Graziano, E., Harland, R., Jessell, T. M., & Edlund, T. (2000). An early requirement for FGF signalling in the acquisition of neural cell fate in the chick embryo. *Curr Biol, 10*(8), 421-429.

Yardley, N., & Garcia-Castro, M. I. (2012). FGF signaling transforms non-neural ectoderm into neural crest. *Dev Biol, 372*(2), 166-177. doi:10.1016/j.ydbio.2012.09.006